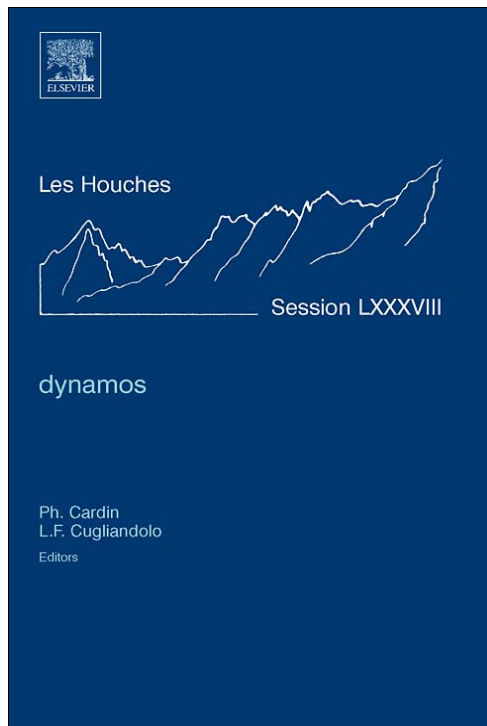


**Provided for non-commercial research and educational use only.
Not for reproduction, distribution or commercial use.**

This chapter was originally published in the book *Les Houches, Session LXXXVIII, 2007, Dynamos*. The copy attached is provided by Elsevier for the author's benefit and for the benefit of the author's institution, for noncommercial research, and educational use. This includes without limitation use in instruction at your institution, distribution to specific colleagues, and providing a copy to your institution's administrator.



All other uses, reproduction and distribution, including without limitation commercial reprints, selling or licensing copies or access, or posting on open internet sites, your personal or institution's website or repository, are prohibited. For exceptions, permission may be sought for such use through Elsevier's permissions site at:

<http://www.elsevier.com/locate/permissionusematerial>

From Anvar Shukurov and Dmitry Sokoloff, *Astrophysical dynamos*. In: Ph. Cardin, L.F. Cugliandolo, editors, *Les Houches, Session LXXXVIII, 2007, Dynamos*.

Amsterdam: Elsevier, 2008, p. 251

ISBN: 978-0-0805-4812-8

© Copyright 2008 Elsevier B.V.

Elsevier

Course 4

ASTROPHYSICAL DYNAMOS

Anvar Shukurov¹ and Dmitry Sokoloff²

¹*School of Mathematics and Statistics, Newcastle University, Newcastle upon Tyne, NE1 7RU, UK*

²*Department of Physics, Moscow State University, Moscow, Moscow, 119992, Russia*

*Ph. Cardin and L.F. Cugliandolo, eds.
Les Houches, Session LXXXVIII, 2007
Dynamos
© 2008 Published by Elsevier B.V.*



Contents

1. Introduction	255
2. Observations of astrophysical magnetic fields	256
2.1. Zeeman splitting	256
2.2. Synchrotron emission and Faraday rotation	258
2.3. Results of observations	260
2.3.1. The Sun and stars	260
2.3.2. Spiral galaxies	261
2.3.3. Galaxy clusters	262
3. Astrophysical flows	265
3.1. Solar convection zone	266
3.2. Spiral galaxies	267
3.2.1. Turbulence and multi-phase structure	267
3.2.2. Galactic rotation	269
3.3. Galaxy clusters	270
4. The necessity of dynamo action	270
5. Dynamo parameters	272
6. Perturbation solutions for mean-field dynamos	273
6.1. Disc dynamos	273
6.1.1. Free decay modes	274
6.1.2. The perturbation expansion	275
6.2. Spherical shell dynamos	279
6.3. Diffusion in mean-field dynamos	282
7. Turbulent magnetic fields in galaxies and galaxy clusters	284
7.1. The fluctuation dynamo	284
7.2. Shapefinders	286
7.3. Turbulence in galaxy clusters: three evolutionary stages	290
7.3.1. The epoch of major mergers	290
7.3.2. Decaying turbulence	291
7.3.3. Turbulent wakes of subclusters and galaxies	292
7.4. Magnetic fields in the intracluster gas	294
7.5. Interstellar turbulent magnetic fields	294
8. Conclusions	295
References	296

Author's personal copy

1. Introduction

The dynamo theory is relatively young: the ability of a flow of conducting fluid to maintain magnetic field was conjectured 90 years ago [23], but the first example of self-sustained dynamo is only 50 years old [17]. Both physical and mathematical aspects of the theory are often complicated and may seem unnatural to an excessively sceptical observer. However, the need for dynamo action to maintain magnetic fields of the Earth and the Sun is so evident (in particular because the global magnetic fields of these objects exhibit time variation that is inconsistent with any other viable option) that the paradigm of dynamo theory has been very widely accepted for planets and stars. The situation is different with other astrophysical objects—accretion discs, galaxies and galaxy clusters. Firstly, magnetic fields in these remote objects are more difficult to detect and explore. Secondly, the size of the parent objects is almost invariably so large (with the exception of accretion discs in stellar objects) that we only have information about the spatial structures of astrophysical magnetic fields and, in vast majority of cases, any time variation can only be hypothesized. Therefore, it is not surprising that, until recently, astrophysical dynamos appeared to be exotic creatures in the world of astrophysics, and the idea of primordial magnetic fields was preferred by many, either explicitly or implicitly. The situation is now changing: more researchers would be prepared to accept that most astrophysical objects host a dynamo as dynamo theory becomes more detailed and capable to provide testable predictions.

Many recent developments in dynamo theory arise from extensive numerical simulations whose complexity approaches, in many respects, that of the laboratory experiment. Therefore, numerical experiments need to be interpreted with the same care and caution as laboratory experiments or astronomical observations. We discuss in Section 7 an approach to quantifying the morphology of (random) structures based on Minkowski functionals. Furthermore, it would be difficult to understand the outcome of complicated models, experiments or observations without a range of simplified analytical models. The recent explosive development of numerical approaches to astrophysical dynamos, based on the growth in the computing power available, has resulted in a reduced interest in simplified analytical models. We believe that this hampers proper interpretation of the numerical results, now often presented in the form of aesthetically appealing images (perhaps arranged into a time sequence called a movie) ac-

accompanied by a subjective qualitative description. We present, in Section 6, a simple but surprisingly accurate analytical approximate solution of the mean-field dynamo equations for thin discs and spherical shells; such solutions can be useful in both interpretations of numerical experiments and in various applications where a simple analytical structure of magnetic field is needed, rather than a three-dimensional data cube.

This text preserves the flavour of lecture notes; in particular, we do not attempt to provide extensive references. The depth of the presentation varies. For example, the reviews of Sections 2–3 only touch upon the observations of astrophysical magnetic fields and the hydrodynamic modelling of stars and galaxies; we only represent facts required to construct solutions of dynamo equations discussed in the second half of the text. We discuss in some detail dynamo models for the Sun, spiral galaxies and galaxy clusters. A review of dynamo action in accretion discs can be found in Refs [9, 41], and dynamos in elliptic galaxies are reviewed in Ref. [41].

We shall be using CGS units in this text, with the unit of magnetic flux density of $1 \text{ G} = 10^{-4} \text{ T}$; in application to galactic magnetic fields, a smaller unit $1 \mu\text{G} = 10^{-6} \text{ G} = 0.1 \text{ nT}$ is often convenient. In the context of stellar physics, the Solar radius $R_{\odot} = 7 \times 10^{10} \text{ cm}$ is a convenient unit length, whereas $1 \text{ pc} = 3 \times 10^{18} \text{ cm} \approx 3.26 \text{ light years}$ is a suitable length scale in the case of galaxies, with $1 \text{ kpc} = 10^3 \text{ pc}$. One parsec is the distance from which the Earth orbit around the Sun has the angular diameter (*parallax*) of one *second* of arc.

2. Observations of astrophysical magnetic fields

2.1. Zeeman splitting

Measuring the splitting of spectral lines in magnetic field is historically the first method of observation of cosmic magnetic fields. Only twelve years after the discovery of Zeeman, Hale [16] has succeeded in using it for measuring the magnetic field of sunspots. Comparison of intensities of a spectral line wings, produced by the Zeeman effect, has allowed Babcock [1] to detect it in the emission of distant peculiar magnetic stars. Ten years later Bolton and Wild [8] proposed to use the Zeeman splitting of the $\lambda 21 \text{ cm}$ neutral hydrogen absorption line to measure magnetic fields in the interstellar medium. Such measurements were achieved a further ten years later [53, 54].

In the absence of external fields, atomic energy levels do not depend on the direction of the total angular momentum (orbital \mathbf{L} plus spin \mathbf{S}) of electrons. In other words, the energy levels are degenerate with respect to the momentum direction. In the magnetic field \mathbf{B} , that distinguishes a certain direction,

an atom acquires the additional energy $-\mu(\mathbf{L} + 2\mathbf{S}) \cdot \mathbf{B}$ which depends on the orientation of the angular momentum with respect to the magnetic field (here, $\mu = e\hbar/2m_e c = 9.3 \times 10^{-21}$ erg G $^{-1}$ is the Bohr magneton). The energy levels split into $2j + 1$ equidistant levels, where j is the quantum number of the total angular momentum $\mathbf{J} = \mathbf{L} + \mathbf{S}$. The energy levels are given by [21]

$$E_H = E_0 \pm \mu g M B, \quad M = 0, 1, \dots, j.$$

The factor g is called the Lande factor,

$$g = 1 + \frac{j(j+1) + s(s+1) - l(l+1)}{2j(j+1)},$$

with l and s the quantum numbers of the orbital and spin momenta. In particular, the Lande factor appears because the mechanical and magnetic momenta are related differently for the electron's orbital motion (M_l, l) and spin (M_s, s): $M_l = -(e/2m_e)l$ and $M_s = -(e/m_e)s$, where m_e is the electron mass.

The quantum selection rules only allow transitions between the levels for which M changes by $\Delta M = 0, \pm 1$. If the Lande factor is the same for the upper and lower levels, the spectral line of the basic frequency ν_0 is split into a triplet (ν_π, ν_σ) (the *normal Zeeman effect*):

$$\nu_\pi = \nu_0, \quad \nu_\sigma = \nu_0 \pm g \frac{e}{4\pi m_e c} B = \nu_0 \pm 1.4 g \left(\frac{B}{10^{-6} \text{ G}} \right) \text{ Hz},$$

where c is the speed of light. In a general case, when the upper and lower levels have different Lande factors the number of components may be larger (the *anomalous Zeeman effect*). The component separation is proportional to the difference in gM between the energy levels involved, $\Delta(gM)$, but remains proportional to magnetic field strength.

The main obstacle in the observations of the Zeeman splitting is the thermal broadening of the spectral lines which can exceed the separation of the multiplet components. For the interstellar $\lambda 21$ cm line of neutral hydrogen, the Zeeman splitting in the field 10^{-5} G is about 30 Hz, while the line half-width due to the thermal Doppler broadening is $\Delta\nu = \nu_0 v_T / c \approx 10^4$ Hz for $T = 100$ K (where v_T is the thermal velocity). Thus, what is often observed in practice is the broadening of spectral lines by the Zeeman effect rather than their splitting. It is therefore important that the components of the spectral lines split by the Zeeman effect are polarized, which helps with their detection because the wings of a spectral line broadened by the Zeeman effect have different polarizations.

In the Solar atmosphere, the Zeeman splitting is observable where magnetic field strength exceeds about 1500 G; magnetic field in sunspots can reach 3000 G. For weaker magnetic fields, polarimetric observations of the Zeeman broadening

are feasible. Detailed discussion of the Zeeman effect and its applications in solar physics can be found in the book of Stix [47]. In the interstellar space the normal Zeeman effect is observed in the $\lambda 21$ cm neutral hydrogen absorption line, and the anomalous Zeeman effect, in the $\lambda 18$ cm OH molecule line. In dense, cold star-forming regions, with gas number density in excess of $n = 10^5\text{--}10^6$ cm $^{-3}$, where magnetic field strength exceeds 1 mG, the Zeeman splitting can be detected in the CO and CN molecular radio lines. At lower densities, the Zeeman broadening of the spectral lines of neutral hydrogen and the hydroxyl OH is observable, but the required gas densities and magnetic fields are still rather high, $n > 10$ cm $^{-3}$, $B > 1$ μ G. These values should be compared with the typical density $n \simeq 0.1$ cm $^{-3}$ in the diffuse warm interstellar medium and $n \simeq 10^{-3}$ cm $^{-3}$ in the hot interstellar gas. Altogether, the Zeeman effect provides the most important method in the observational studies of the Solar magnetic fields and plays prominent role in the observations of magnetic fields of other stars. In the interstellar space, however, this method is useful only when applied to relatively dense regions with rather strong magnetic fields. Although interstellar gas clouds are the site of many important processes (including star formation), they occupy a negligible fraction of the total volume of the interstellar space.

2.2. Synchrotron emission and Faraday rotation

Estimates of magnetic field strength in the diffuse interstellar medium of the Milky Way and other galaxies are most efficiently obtained from the intensity and Faraday rotation of synchrotron emission. The total I and polarized P synchrotron intensities and the Faraday rotation measure RM are weighted integrals of magnetic field over the path length L from the source to the observer, so they provide various average measures of magnetic field in the emitting or magneto-active volume:

$$I = K \int_L n_{\text{cr}} B_{\perp}^2 ds, \quad P = K \int_L n_{\text{cr}} \bar{B}_{\perp}^2 ds, \quad \text{RM} = K_1 \int_L n_e B_{\parallel} ds, \quad (2.1)$$

where n_{cr} and n_e are the number densities of relativistic and thermal electrons, $\mathbf{B} = \bar{\mathbf{B}} + \mathbf{b}$ is the total magnetic field comprising regular $\bar{\mathbf{B}}$ and random \mathbf{b} parts, with $\bar{\mathbf{B}} = \langle \mathbf{B} \rangle$, $\langle \mathbf{b} \rangle = 0$ and $\langle B^2 \rangle = \langle B \rangle^2 + \langle b^2 \rangle$, where angular brackets denote averaging, subscripts \perp and \parallel refer to magnetic field components perpendicular and parallel to the line of sight, and K and $K_1 = e^3/(2\pi m_e^2 c^4) = 0.81$ rad m $^{-2}$ cm 3 μ G $^{-1}$ pc $^{-1}$ are certain dimensional constants (an explicit expression for K is omitted here; it can be found, e.g., in Ref. [27]). The degree of polarization p is related to the degree of regularity of the magnetic field. In the

simplest case of $n_{\text{cr}} = \text{const}$, an expression often used is

$$p \equiv \frac{P}{I} \approx p_0 \frac{\bar{B}_\perp^2}{\langle B_\perp^2 \rangle} = p_0 \frac{\bar{B}_\perp^2}{\bar{B}_\perp^2 + \frac{2}{3} \langle b^2 \rangle}, \quad (2.2)$$

where the random field \mathbf{b} has been assumed to be isotropic in the last equality, and $p_0 \approx 0.75$ weakly depends on the spectral index of the emission. This widely used relation is only approximate. In particular, it does not allow for any anisotropy of the random magnetic field, for the dependence of n_{cr} on B , and for depolarization effects; some generalizations are discussed in Ref. [44].

The orientation of the apparent large-scale magnetic field in the sky plane is given by the observed B -vector of the polarized synchrotron emission. As polarized radio emission propagates through magnetized plasma, its polarization plane rotates because of what is known as the Faraday effect (i.e., magnetized plasma is birefringent). The rotation angle is given by $\Delta\psi = \text{RM} \lambda^2$, where λ is the emission wavelength. The Faraday rotation measure can be obtained from measurements of the differences in the polarization angles ψ between several wavelengths. The special importance of the Faraday rotation measure, RM, is that this observable is sensitive to the direction of \mathbf{B} (the sign of \bar{B}_\parallel) and this allows one to determine not only the orientation of \mathbf{B} but also its direction. Thus, analysis of Faraday rotation measures can reveal the three-dimensional structure of the magnetic vector field.

Since n_{cr} is difficult to measure, it is often assumed that magnetic field and cosmic rays are in pressure equilibrium or energy equipartition; this allows to express n_{cr} in terms of B . The physical basis of this assumption is the fact that cosmic rays (charged particles of relativistic energies) are confined by magnetic fields. The cosmic ray number density n_{cr} in the Milky Way can be determined independently from the γ -ray emission produced when cosmic ray particles interact with the interstellar gas [48]. Then magnetic field strength can be obtained without assuming equipartition; the results are generally consistent with the equipartition values.

In the Milky Way, the dispersion measures of pulsars, $\text{DM} = \int_L n_e ds$ provide information about the mean thermal electron density, but the accuracy is limited by our uncertain knowledge of distances to pulsars. Estimates of the strength of the regular magnetic field in the Milky Way are often obtained from the Faraday rotation measures of pulsars simply as

$$\bar{B}_\parallel = \frac{\text{RM}}{K_1 \text{DM}}. \quad (2.3)$$

This estimate is meaningful if magnetic field and thermal electron density are statistically uncorrelated. If the fluctuations in magnetic field and thermal electron

density are correlated with each other, they will contribute positively to RM and Eq. (2.3) will yield overestimated \bar{B}_{\parallel} . In the case of anticorrelated fluctuations, their contribution is negative and Eq. (2.3) is an underestimate. Physically reasonable assumptions about the statistical relation between magnetic field strength and electron density can lead to Eq. (2.3) being in error by a factor of 2–3 [5].

Magnetic fields in the Solar corona can also be measured via their rotation of the polarization plane of the radio emission of background extragalactic radio sources [46]. At the wavelength of $\lambda 21$ cm, a magnetic field of 0.03 G in the corona (thermal electron density of $1.5 \times 10^4 \text{ cm}^{-3}$, path length of ten solar radii) produces $\text{RM} \simeq 10 \text{ rad m}^{-2}$, with the corresponding rotation angle of the polarization plane of 25° .

2.3. Results of observations

2.3.1. The Sun and stars

The magnetic fields that are most readily observable in the Sun are those in the sunspots, where magnetic fields of a strength exceeding 1500 G makes the Zeeman spectral multiplets observable. Weaker fields are detectable through the Zeeman broadening. Despite strong local magnetic fluctuations associated with the granulation, a weaker overall magnetic field of the Sun can be measured; it is dominated by a dipolar component of a strength 1 G near the poles. The overall magnetic field is oscillatory with a period of about 22 years, and is described as a dynamo wave propagating from latitudes $\pm(30^\circ\text{--}35^\circ)$ towards the Solar equator down to the latitude of about $\pm(5^\circ\text{--}10^\circ)$ in each hemisphere; an additional, weaker branch of the dynamo wave propagates polewards from the mid-latitudes. The strong magnetic field of the sunspots is believed to be a surface manifestation of the strong toroidal magnetic field produced in the Solar interior. Unlike the dipolar poloidal magnetic field, the overall toroidal magnetic field does not penetrate outside the Solar surface (except in the sunspots), in agreement with the vacuum boundary conditions often employed in modelling the large-scale magnetic field of the Sun. The overall symmetry of the Solar magnetic field is approximately dipolar, $\bar{B}_r(\theta) = -\bar{B}_r(-\theta)$, $\bar{B}_\theta(\theta) = \bar{B}_\theta(-\theta)$, $\bar{B}_\phi(\theta) = -\bar{B}_\phi(-\theta)$ in terms of spherical coordinates with θ the latitude ($\theta = 0$ at the equator and $\theta = \pm 90^\circ$ at the poles). Although weak, deviations from the perfect equatorial antisymmetry and axial symmetry are noticeable; these are described as a quadrupolar component of the magnetic field and ‘active longitudes’.

Magnetic fields in other stars can be detected using various proxies. For example, spectral lines of ionized oxygen and calcium, O VI and Ca II are produced in the magnetically heated plasmas in the chromosphere. The emission flux in these lines is known to be proportional to the square root of the magnetic field strength.

Observations in these lines reveal stellar activity cycles in late-type stars G0–K7, which have an outer convection zone. Magnetic activity cycles result in a cyclic variation of the area covered by starspots, and hence to cyclic photometric variations; the techniques of Doppler imaging allow the production of maps of the stellar surface showing large starspots [29].

2.3.2. Spiral galaxies

The observable quantities (2.1) have provided extensive data on magnetic field strengths in both the Milky Way and external galaxies. The average total field strengths in nearby spiral galaxies, obtained from total synchrotron intensity I , ranges from $B \approx 4 \mu\text{G}$ in the galaxy M31 to about $15 \mu\text{G}$ in M51, with a mean of $B = 9 \mu\text{G}$ for the sample of 74 galaxies [2]. The typical degree of polarization of synchrotron emission from galaxies at short radio wavelengths is $p = 10\text{--}20\%$, so Eq. (2.2) gives $\bar{B}/B = 0.4\text{--}0.5$; these are always lower limits due to the limited resolution of the observations, and $\bar{B}/B = 0.6\text{--}0.7$ is a more plausible estimate. The total equipartition magnetic field in the Solar neighbourhood is estimated as $B = 6 \pm 2 \mu\text{G}$ from the synchrotron intensity of the diffuse Galactic radio background. Combined with $\bar{B}/B = 0.65$, this yields a strength of the local regular field of $\bar{B} = 4 \pm 1 \mu\text{G}$. Hence, the typical strength of the local Galactic random magnetic fields, $b = (B^2 - \bar{B}^2)^{1/2} = 5 \pm 2 \mu\text{G}$, exceeds that of the regular field by a factor $b/\bar{B} = 1.3 \pm 0.6$. RM data yield similar values for this ratio.

Meanwhile, the values of \bar{B} in the Milky Way obtained from Faraday rotation measures seem to be systematically lower than the above values. RM of pulsars and extragalactic radio sources yield $\bar{B} = 1\text{--}2 \mu\text{G}$ in the solar vicinity, a value about twice smaller than that inferred from the synchrotron intensity and polarization. The discrepancy can be explained, at least in part, if the methods described above sample different volumes. The depth probed by the total synchrotron emission and Faraday rotation measures of pulsars and extragalactic radio sources is of the order of a few kpc. Polarized emission, however, may emerge from more nearby regions because emission from remote regions is *depolarized* by various propagation effects [44]. However, a more fundamental reason for the discrepancy can be a partial correlation between fluctuations in magnetic field and thermal electron density. Such a correlation can arise from statistical pressure balance in the interstellar medium: if the total pressure is constant on average, regions with larger gas density (and hence larger gas pressure) usually have weaker magnetic field (and hence lower magnetic pressure), and vice versa. The term $\langle b_{\parallel} n_e \rangle$ then differs from zero and contributes to the observed RM leading to underestimated \bar{B} [5]. In a similar manner, correlation between B and the cosmic ray number density n_{cr} biases the estimates of magnetic field from synchrotron intensity and polarization [44]. Altogether, $\bar{B} = 4 \mu\text{G}$ and $b = 5 \mu\text{G}$

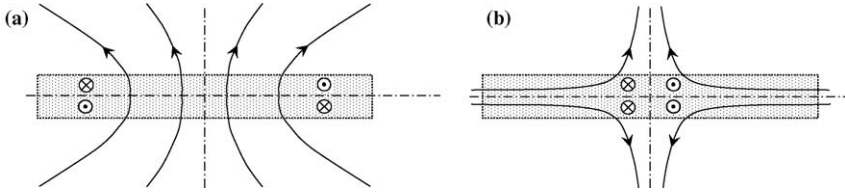


Fig. 1. A schematic representation of the magnetic lines of the meridional magnetic field (solid) of (a) dipolar and (b) quadrupolar symmetry in a thin disc (shaded). The direction of the azimuthal magnetic field on both sides of the slab's midplane is also shown: \odot , out of the page and \otimes , into the page. The symmetry remains unchanged if all the field directions are simultaneously reversed.

seem to be acceptable estimates of magnetic field strengths for a region within several kiloparsecs from the Sun.

Unlike the Solar magnetic field, which has a dipolar parity, galactic magnetic fields appear to be *quadrupolar* [13]; the difference is illustrated in Fig. 1. This general fact that the global magnetic fields of spherical objects (including stars and planets) are likely to be predominantly dipolar, whereas those of flat objects (spiral galaxies) are quadrupolar can be elegantly explained by the dynamo theory (see Sect. 6.1.2).

To summarize, magnetic fields of spiral galaxies have the following typical parameters. At scales much larger than the turbulent scale of about 100 pc, the strength of the global magnetic field is $\bar{B} \simeq 3\text{--}7 \mu\text{G}$. With the total field strength of $B \simeq 5\text{--}12 \mu\text{G}$, the ratio of energy densities in the random and regular magnetic fields is $\langle b^2 \rangle / \bar{B}^2 \simeq 3$. The global magnetic field is likely to have a global quadrupolar parity, but this has been verified observationally only for the Milky Way. The global magnetic pattern has the form of a spiral trailing with respect to the galactic rotation (similarly to the galactic spiral arms), with the pitch angle $p_B = \arctan \bar{B}_r / \bar{B}_\phi = -(10^\circ\text{--}30^\circ)$. Galactic magnetic fields exhibit a variety of complicated spatial structures (e.g., magnetic arms, field reversals between the disc and the halo, etc.). There is a widespread misconception that the strength of the regular magnetic field near the Sun, $\bar{B}_\odot \approx 2 \mu\text{G}$, is representative of all spiral galaxies. In fact, the Sun is close to a reversal of the large-scale magnetic field; magnetic fields at smaller galactocentric radii are significantly stronger than that in the immediate vicinity of the Sun.

2.3.3. Galaxy clusters

Galaxy clusters are the largest gravitationally bound systems in the universe, having masses of order $10^{14}\text{--}10^{15} M_\odot$. Observations of clusters in X-rays reveal that they have an atmosphere of hot gas with temperatures $T \simeq 10^7\text{--}10^8$ K, extend-

ing over scales of order 1 Mpc = 10^6 pc. Succinct reviews of the observational data on cluster magnetic fields can be found in Refs [10, 15]. The central parts of a relatively small fraction of galaxy clusters emit radio synchrotron emission (i.e., possess radio halos) which directly indicates the presence of magnetic fields and relativistic electrons in their intergalactic medium. Cluster magnetic fields can also be probed using Faraday rotation studies of both cluster radio galaxies and background radio sources seen through the cluster. Clear contribution of the intracluster medium to the Faraday rotation has been detected in many clusters, so that it seems plausible that magnetic fields (unlike relativistic electrons) are common in clusters of galaxies.

Typical number density and temperature of the interstellar gas of such rich galaxy clusters as Coma are $n = 10^{-3} \text{ cm}^{-3}$ and $T = 10^6 \text{ K}$. The radius of the synchrotron halo in Coma is $L \simeq 500 \text{ kpc}$. Under the assumption of energy equipartition between the cosmic rays and magnetic fields, magnetic field strength is of order $2 \mu\text{G}$. Over the path length $L = 500 \text{ kpc}$, such a field would produce $\text{RM} \simeq 10^3 \text{ rad m}^{-2}$. However, the observed RM is ten times smaller being of order 100 rad m^{-2} [11]. The difference is explained by the fact that magnetic field is random. To justify this, we consider the autocorrelation function of the Faraday rotation measure in a random magnetic field. For this purpose, we introduce coordinates (x, y, z) with the z -axis directed towards the observer, and those in the plane of the sky, $\mathbf{X} = (X, Y)$. We assume the magnetic field to be an isotropic, homogeneous, random field with zero mean value. Then its equal-time, two-point correlation tensor has the form $\langle B_i(\mathbf{x}, t) B_j(\mathbf{y}, t) \rangle = M_{ij}(r, t)$, where

$$M_{ij} = \left(\delta_{ij} - \frac{r_i r_j}{r^2} \right) M_N(r, t) + \frac{r_i r_j}{r^2} M_L(r, t).$$

Here $r = |\mathbf{x} - \mathbf{y}|$, $r_i = x_i - y_i$; $M_L(r, t)$ and $M_N(r, t)$ are known as the longitudinal and transverse correlation functions of the magnetic field, respectively ([26]; Section 34 of [22]). Since $\nabla \cdot \mathbf{B} = 0$,

$$M_N = \frac{1}{2r} \frac{\partial}{\partial r} (r^2 M_L).$$

We further assume for simplicity that the electron density is constant. This is consistent with the fact that random gas motions in galaxy clusters are quite subsonic. The correlation function of RM is then

$$\begin{aligned} C(R) &= \langle \text{RM}(\mathbf{X}_1) \text{RM}(\mathbf{X}_2) \rangle \\ &= K_1^2 n_e^2 \int_0^L \int_0^L B_z(\mathbf{X}_1, z_1) B_z(\mathbf{X}_2, z_2) dz_1 dz_2 \end{aligned}$$

$$\begin{aligned}
 &= K_1^2 n_e^2 L \int_{-L}^L M_{zz}(R, \zeta) d\zeta \\
 &= K_1^2 n_e^2 L \int_{-L}^L \left(M_N \frac{R^2}{R^2 + \zeta^2} + M_L \frac{\zeta^2}{R^2 + \zeta^2} \right) d\zeta \\
 &= K_1^2 n_e^2 L \int_{-L}^L \left(M_L + \frac{R^2}{2r} \frac{dM_L}{dr} \right) d\zeta. \tag{2.4}
 \end{aligned}$$

Here we have assumed that L is much larger than the correlation length of the magnetic field, $\zeta = z_1 - z_2$, $R = |\mathbf{X}_1 - \mathbf{X}_2|$ and $r^2 = R^2 + \zeta^2$.

For the sake of illustration, consider the longitudinal correlation function of the form

$$M_L = \frac{1}{3} b^2 \exp\left(-\frac{r^2}{2l_B^2}\right),$$

which corresponds to the one-dimensional magnetic spectrum of the form $M_k \propto k^4 \exp(-k^2 l_B^2 / 2)$ [26]; here $b^2 = \langle B^2 \rangle$. We note that M_k attains maximum at a wavenumber $k_m = 2/l_B$ (or a scale $2\pi/k_m = \pi l_B$), whereas the longitudinal correlation scale is given by $l_L = [M_L(0)]^{-1} \int_0^\infty M_L(r) dr = l_B \sqrt{\pi/2}$.

Straightforward calculation then yields

$$C(R) = \frac{\sqrt{2\pi}}{3} K_1^2 n_e^2 b^2 L l_B \left(1 - \frac{R^2}{2l_B^2}\right) \exp\left(-\frac{R^2}{2l_B^2}\right). \tag{2.5}$$

The root-mean-square value of RM can be obtained from Eq. (2.4) or (2.5) at $R = 0$:

$$\sigma_{\text{RM}}^2 = K_1^2 n_e^2 L \int_{-L}^L M_L(R, \zeta)|_{R=0} d\zeta = \frac{\sqrt{2\pi}}{3} K_1^2 n_e^2 b^2 L l_B. \tag{2.6}$$

Thus, the standard deviation of RM grows with the square root of the path length L , $\sigma_{\text{RM}} \propto L^{1/2}$. This happens because the polarization angle ψ of the radio emission propagating through the random magnetic field experiences random walk because of the Faraday rotation, and hence the amount of rotation accumulated is proportional to $N^{1/2}$, where $N \simeq L/l_B$ is the number of correlation cells on the path length. Since $\text{RM} \propto \Delta\psi$, where $\Delta\psi$ is the difference in ψ between two wavelengths, the resulting standard deviation of RM is also proportional to $N^{1/2}$. If the value of RM produced in a single correlation cell is $\text{RM}_0 \simeq K_1 n_e b l_B$, we obtain $\sigma_{\text{RM}} \simeq \text{RM}_0 N^{1/2}$, which agrees with Eq. (2.6).

Using $b = 2 \mu\text{G}$, $n_e = 10^{-3} \text{ cm}^{-3}$, $L = 500 \text{ kpc}$ and $\sigma_{\text{RM}} = 100 \text{ rad m}^{-2}$ in Eq. (2.6), we obtain the magnetic correlation length as $l_B \simeq 10 \text{ kpc}$. Thus, the correlation length of magnetic fields in the intracluster gas of galaxy clusters

is much smaller than the size of a cluster (but is rather comparable to the size of a galaxy). An estimate of the field strength in galaxy clusters obtained from Faraday rotation measurements is [11]

$$b \simeq 5(l_B/10 \text{ kpc})^{-1/2} \mu\text{G}.$$

In conclusion, there is considerable evidence that galaxy clusters are magnetized with the field root-mean-square strength ranging from a few μG to several tens of μG in the central parts of some clusters, and with coherence scales of order 10 kpc. These fields, if not maintained by some mechanism, will evolve as decaying MHD turbulence, and perhaps decay on the appropriate Alfvén time scale of about 10^8 yr, much shorter than the age of the cluster. Even though the scale of the magnetic field is comparable to the size of a galaxy, these magnetic fields cannot result from stripping of the interstellar gas together with its magnetic field: the strength of any magnetic field stripped from a galaxy decreases by a factor of order ten as the gas expands from the interstellar densities of order 0.1 cm^{-3} to the intergalactic densities of about 10^{-3} cm^{-3} : $B \propto n^{2/3}$ if magnetic field is frozen into the gas and the expansion is spherically symmetric. Thus, even under optimistic assumptions the stripping could account for at most 0.1 of the observed intergalactic magnetic field strength. Magnetic fields in galaxy clusters need dynamo action to be produced [32, 50].

3. Astrophysical flows

As discussed elsewhere in this volume, the generation of a magnetic field at a scale comparable to the size of the parent object is a rather subtle process: since the regular magnetic field is not mirror symmetric, its generation is a symmetry-breaking process. (If the magnetic field is of a small scale, the system remains mirror-symmetric on the average, and no systematic deviations from the mirror symmetry are required to maintain a small-scale magnetic field—see Sect. 7.) To appreciate the significance of mirror symmetry, look at the face of a clock through a mirror. The numbers on the dial's reflection look differently from the original. However, the sense of rotation of the hands is the same in the clock and in its mirror image. Under a mirror reflection of the Cartesian reference frame, $(x, y, z) \rightarrow (x, y, -z)$, the velocity components transform similarly, $(v_x, v_y, v_z) \rightarrow (v_x, v_y, -v_z)$, and so the linear velocity \mathbf{v} is a true vector. But the angular velocity or vorticity $\boldsymbol{\omega} = \nabla \times \mathbf{v}$ change differently under the reflection, $(\omega_x, \omega_y, \omega_z) \rightarrow (-\omega_x, -\omega_y, \omega_z)$, and so these vector fields are *not* mirror-symmetric. [Write out the vorticity components in terms of the partial derivatives of v_x, v_y, v_z to obtain the above symmetry relations from those for \mathbf{r} and \mathbf{v} .] The

angular velocity is a *pseudo*-vector. Magnetic field is a pseudo-vector too: consider the reflections of a linear electric current \mathbf{j} and the associated magnetic field \mathbf{B} , with $\mathbf{j} = \nabla \times \mathbf{B}$. Similarly, helicity of motion $\mathbf{v} \cdot \boldsymbol{\omega}$ is a pseudo-scalar as it changes sign upon mirror reflection (indeed, the reflection of a right-handed screw is a left-handed screw).

The mirror asymmetry of the magnetic field has far-reaching physical consequences: a system that is perfectly mirror symmetric (i.e., lacks any pseudo-vectorial or pseudo-scalar properties) cannot generate magnetic field at its own scale. A pseudo-vectorial property ubiquitous in astrophysical systems is rotation, resulting in the intrinsic connection of regular magnetic fields and rotation.

Another feature of electrically conducting flows important for magnetic fields is the randomness or Lagrangian chaos: the trajectories of elementary volumes in a random or chaotic flows diverge exponentially. In a fluid of high electric conductivity, magnetic field is (almost) frozen into the flow, and the divergence of the trajectories can lead to the exponential stretching and, therefore, exponential amplification of magnetic field embedded into the flow. A type of randomness widespread in nature is turbulence; hence, the importance of turbulent dynamos.

In this section we briefly discuss the properties of plasma motions in the Sun, spiral galaxies and galaxy clusters important for the generation of magnetic fields. Our focus will be on differential rotation, the α parameter of small-scale random motions (a measure of their deviation from mirror symmetry) and turbulent magnetic diffusivity.

3.1. Solar convection zone

The Sun's magnetic field is maintained by convective motions in its part known as the convection zone which extends from a radius of $0.7R_{\odot}$ to about $0.95R_{\odot}$ (almost the Solar surface). The angular velocity of rotation in the convection zone has been determined using methods of helioseismology. The angular velocity slightly increases with the radius within about 30° of the equator and decreases closer to the poles. With the mean angular velocity of $\Omega \simeq 4.6 \times 10^{-6} \text{ s}^{-1}$, the magnitude of the differential rotation across the convection zone is $\Delta\Omega \simeq 0.1\Omega$. A thin region between the convection zone and the radiative zone, known as the tachocline, is a site of especially strong differential rotation; this makes this region especially important for the solar dynamo [18].

The scale and velocity of the convective motions associated with the granulation are $l \simeq 10^3 \text{ km}$ and $v \simeq 1 \text{ km s}^{-1}$, respectively. With the granulation time scale $\tau \simeq 500 \text{ s} \approx 10 \text{ min}$, the Rossby number of these motions is $\text{Ro} = (2\Omega\tau)^{-1} \simeq 300$. Convective structures of a larger scale, mesogranules, have $l \simeq 3.5 \times 10^4 \text{ km}$, $v \simeq 0.5 \text{ km s}^{-1}$, $\tau \simeq 5 \times 10^4 \text{ s}$ and $\text{Ro} \simeq 3$. For the deep convection zone, the relevant parameters are: the pressure scale

height $h \simeq 5 \times 10^9$ cm, the gas density $\rho \simeq 0.2 \text{ g cm}^{-3}$, and the convection velocity $v \simeq 20 \text{ m s}^{-1}$ and scale $l \simeq 2 \times 10^9$ cm. Magnetic field strength corresponding to energy equipartition with the kinetic energy of the convection is $B = (4\pi\rho v^2)^{1/2} \simeq 3000 \text{ G}$, and the Rossby number is $\text{Ro} \simeq 0.6$. The relatively small value of the Rossby number indicates that convective motions deep in the convection zone are significantly modified by rotation; in particular, they acquire significant helicity.

3.2. Spiral galaxies

3.2.1. Turbulence and multi-phase structure

The interstellar medium (ISM) is much more inhomogeneous and active than stellar and planetary interiors. The reason for that is ongoing star formation: massive young stars evolve rapidly (in about 10^6 yr) and then explode as supernova stars (SN) releasing large amounts of energy ($E_{\text{SN}} \simeq 10^{51}$ erg per event). These explosions control the structure of the ISM.

SN remnants are filled with hot, overpressured gas that starts by expanding supersonically; at this stage the gas surrounding the blast wave is not perturbed. When pressure inside a SN remnant reduces to values comparable to that in the surrounding gas, the remnant disintegrates and merges with the ISM—at this stage the expanding SN remnant drives motions in the surrounding gas, and its energy is partially converted into the kinetic energy of the ISM. Since SN occur at (almost) random times and positions, the result is a random force that drives random motions in the ISM, which eventually become turbulent. The size of an SN remnant when it has reached pressure balance, determines the energy-range turbulent scale,

$$l \simeq 0.05\text{--}0.1 \text{ kpc}.$$

A fraction $f = 0.07$ of the SN energy is converted into the ISM's kinetic energy. With the SN frequency of $\nu_{\text{SN}} \sim (30 \text{ yr})^{-1}$ in the Milky Way (i.e., one SN per 30 yr), the kinetic energy supply rate per unit mass is $\dot{e}_{\text{SN}} = f\nu_{\text{SN}}E_{\text{SN}}M_{\text{gas}}^{-1} \sim 10^{-2} \text{ erg g}^{-1} \text{ s}^{-1}$, where $M_{\text{gas}} = 4 \times 10^9 M_{\odot}$ is the total mass of gas in the galaxy. This energy supply can drive turbulent motions at a speed v such that $2v^3/l = \dot{e}_{\text{SN}}$ (where the factor 2 allows for equal contributions of kinetic and magnetic turbulent energies), which yields

$$v \simeq 10\text{--}30 \text{ km s}^{-1},$$

a value similar to the speed of sound at a temperature $T = 10^4 \text{ K}$ or higher. The corresponding turbulent diffusivity follows as

$$\eta_t \simeq \frac{1}{3}lv \simeq (0.5\text{--}3) \times 10^{26} \text{ cm}^2 \text{ s}^{-1}. \quad (3.1)$$

Supernovae are the main source of turbulence in the ISM. Stellar winds is another significant source, contributing about 25% of the total energy supply.

The time interval between supernova shocks passing through a given point is about [24]

$$\tau = (0.5-5) \times 10^6 \text{ yr.}$$

After this period of time, the velocity field at a given position completely renovates to become independent of its previous form. Therefore, this time can be identified with the correlation time of interstellar turbulence. The renovation time is 2–20 times shorter than the ‘eddy turnover’ time $l/v \simeq 10^7$ yr. This means that the short-correlated (or δ -correlated) approximation, so often employed in turbulence and dynamo theory, can be quite accurate in application to the ISM—this is a unique feature of the interstellar turbulence. Note that the standard estimate (3.1) is valid if the correlation time is l/v . If the renovation time was used instead, the result would be $\eta_t \simeq l^2/\tau \simeq 10^{27} \text{ cm}^2 \text{ s}^{-1}$, a value an order of magnitude larger than the standard estimate.

Another important result of supernova activity is a large amount of gas heated to a temperature $T = 10^6$ K. The gas is so tenuous that the collision rate of the gas particles is low, and so its radiative cooling time is very long and exceeds τ : the hot bubbles produced by supernovae can merge before they cool. The result is a network of hot tunnels that form the hot component of the ISM. Altogether, the interstellar gas is found in several distinct states, known as ‘phases’ (this usage may be misleading as most of them are not proper thermodynamic phases) whose parameters are presented in Table 1. Some of the parameters (especially the volume filling factors) are not known confidently, so estimates of Table 1 should be approached with healthy caution. The warm diffuse gas can be considered as a background against which the ISM dynamics evolves; this is the primary phase that occupies a connected (percolating) region in the disc, whereas the hot gas

Table 1

The multi-phase ISM. The origin and parameters of the most important phases of interstellar gas: n , the mid-plane number density in hydrogen atoms per cm^3 ; T , the temperature in K; c_s , the speed of sound in km s^{-1} ; h , the scale height in kpc; and f_V , the volume filling factor in the disc of the Milky Way, in percent

Phase	Origin	n	T	c_s	h	f_V
Warm		0.1	10^4	10	0.5	60–80
Hot	Supernovae	10^{-3}	10^6	100	3	20–40
Hydrogen clouds	Compression	20	10^2	1	0.1	2
Molecular clouds	Self-gravity, thermal instability	10^3	10	0.3	0.075	0.1

may or may not fill a connected region. The warm gas is ionized by the stellar ultraviolet radiation and cosmic rays; its degree of ionization is about 30% at the Galactic midplane. The hot gas is so hot that it is fully ionized by gas particle collisions.

The locations of SN stars are not entirely random: 70% of them cluster in regions of intense star formation (known as OB associations as they contain large numbers of young, bright stars of spectral classes O and B) where gas density is larger than on average in the galaxy. Collective energy input from a few tens (typically, 50) of SN within a region about 0.5–1 kpc in size produces a superbubble that can break through the galactic disc. This removes the hot gas into the galactic halo and significantly reduces its filling factor in the disc (from about 70% to 10–20%). This also gives rise to a systematic outflow of the hot gas to large heights where the gas eventually cools, condenses and returns to the disc after about 10^9 yr in the form of cold, dense clouds of neutral hydrogen. This convection-type flow is known as the galactic fountain, and it can plausibly support a mean-field dynamo of its own [45]. The local vertical velocity of the hot gas at the base of the fountain flow is 100–200 km s⁻¹. Thus, galactic discs are open systems that exchange matter and magnetic fields with the galactic halos (cf. [20]). This exchange can be important for the magnetic helicity balance and galactic dynamo action [42].

3.2.2. Galactic rotation

Spiral galaxies have conspicuous flat components because they rotate rapidly enough. The Sun moves in the Milky Way at a velocity of about $V_{\odot} = r_{\odot}\Omega_{\odot} = 220$ km s⁻¹, to complete one orbit of a radius $r_{\odot} \approx 8.5$ kpc in $2\pi/\Omega_{\odot} = 2.4 \times 10^8$ yr. These values are representative for spiral galaxies in general. The Rossby number is estimated as

$$\text{Ro} = \frac{v}{l\Omega_{\odot}} \sim 4.$$

$\text{Ro} = 1$ at a scale 0.4 kpc in the warm gas, which is similar to the scale height of the gas layer. This implies that rotation significantly affects turbulent gas motions, making them helical on average, so that they are capable of producing large-scale magnetic fields via the α -effect of the mean-field dynamo theory. A convenient estimate of the α -effect can be obtained from Krause's formula,

$$\alpha_0 \simeq \frac{l^2\Omega}{h} \approx 0.5 \text{ km s}^{-1}, \quad (3.2)$$

where Ω is the angular velocity, and the numerical estimate refers to the Solar neighbourhood of the Milky Way. Thus, $\alpha_0 \simeq 0.05v$ near the Sun and increases in the inner Galaxy together with Ω . This estimate of α_0 will be used to calculate

the dynamo number and, hence, to assess the efficiency of dynamo action in the Galaxy.

The spatial distribution of galactic rotation is known for thousands galaxies [43] from systematic Doppler shifts of various spectral lines emitted by stars and gas. In this respect, galaxies are much better explored than any star or planet (including the Sun and the Earth) where reliable data on the angular velocity in the interior are much less detailed and reliable or even unavailable. The radial profile of the galactic rotational velocity is called the rotation curve. Rotation curves of most galaxies are flat beyond a certain distance from the axis, so $\Omega \propto r^{-1}$ is a good approximation for $r \gtrsim 5$ kpc.

3.3. *Galaxy clusters*

Clusters of galaxies do not exhibit any rotation. Correspondingly, magnetic field in the intracluster gas is random, without any mean component. Theoretical models strongly suggest that the intracluster gas is turbulent [12, 50]. The turbulence is mainly driven by the recent or ongoing merger events where large clumps of matter merge to form the cluster. The scale and velocity of the turbulent motions are estimated as $l \simeq 250\text{--}150$ kpc and $v \simeq 300\text{--}150$ km s⁻¹; the latter is useful to compare with the speed of sound (or the thermal velocity) in the gas, $c_s \approx 1000$ km s⁻¹. Since the turbulent Mach number is as small as 0.3 or even less, the compressibility effects are relatively weak and the turbulent fluctuations in the gas density can be neglected. The intracluster plasma is so tenuous that the mean free path is of order 10 kpc. Nevertheless, magnetohydrodynamic description remains meaningful because, in a magnetized plasma, the role of the mean free path is played by the Larmor radius which is very small even in magnetic fields much weaker than those observed in galaxy clusters. However, the corresponding effective pressure becomes anisotropic, and this can lead to interesting (and largely unexplored) effects [35].

4. **The necessity of dynamo action**

The necessity of dynamo action in the Earth and the Sun is practically obvious, in part because of the time variation of the magnetic fields of these objects: the geomagnetic magnetic field is known to change its polarity at irregular time intervals, whereas the solar magnetic field drives the 11-year activity cycle and changes its polarity every 22 years. Even without any other arguments in favour of planetary and stellar dynamos, the time variation would be sufficient to treat seriously applications of dynamo theory to planets and stars.

The situation is different with galaxies where the time scales involved are by far too long to be useful for this purpose and the only clues to the origin of

galactic magnetic fields come from their spatial structures. Nevertheless, there are several lines of evidence that consistently indicate that the large-scale galactic magnetic fields need to be maintained by ongoing dynamo action [41] (see, however, [20]).

It is sometimes claimed that magnetic field does not need any support if the electric resistivity of the medium is small enough, i.e., the magnetic Reynolds number is large enough. In the case of the interstellar gas, the magnetic diffusivity of a fully ionized gas, $\eta = 10^7 (T/10^4 \text{ K})^{-3/2} \text{ cm}^2 \text{ s}^{-1}$, is so small that the magnetic Reynolds number at the scale equal to the scale height of the warm gas $h = 500 \text{ pc}$ is as large as $R_m \simeq 10^{20}$, and the decay time of the large-scale magnetic field would seem to follow as 10^{27} yr . However, this estimate is hardly useful because the ISM is turbulent, and the corresponding decay time of the large-scale magnetic field is only $h^2/\eta_t \simeq 5 \times 10^8 \text{ yr}$. More generally, since magnetic energy in any three-dimensional turbulent flow rapidly cascades towards small scales where it dissipates, any three-dimensional, turbulent, magnetized system needs some form of dynamo action to maintain its magnetic field in a steady state.

Another argument in favour of dynamo action is related to the fact that the large-scale magnetic fields of spiral galaxies are only mildly wrapped up by the differential rotation, with the pitch angle $p_B = \arctan \bar{B}_r/\bar{B}_\phi = -(10^\circ-30^\circ)$, where the negative sign means that the magnetic spiral is trailing with respect to the galactic rotation. Near the Sun, the Milky Way galaxy gas made about $N = 30$ (differential) rotations during its lifetime. If the galactic large-scale magnetic field was primordial and its spiral shape was produced by the differential rotation, its pitch angle would be of the order of $p_B \simeq -1/N \simeq -2^\circ$. This suggests that the large-scale magnetic field observed in the Milky Way and in spiral galaxies in general cannot be just a primordial magnetic field twisted by differential rotation.

If an external, quasi-uniform magnetic field is to have quadrupolar symmetry with the respect to the disc's midplane, as appropriate to spiral galaxies, it has to be in the plane of the galaxy. Then an initially (quasi-)uniform magnetic field would be twisted into a nonaxisymmetric configuration with the azimuthal wave number $m = 1$ (a bisymmetric structure). Meanwhile, dynamo models in a thin disc consistently favour axially symmetric magnetic structures, $m = 0$. Early observations of galactic magnetic fields seemed to indicate that the global magnetic structures are predominantly bisymmetric, in contradiction with the galactic dynamo theory. However, the improved quality of observations and their interpretation since the 1990's have unexpectedly revealed that magnetic structures in most (if not all) spiral galaxies can be described as variously distorted axisymmetric magnetic fields [4]: what seemed to be a weakness of the dynamo theory turned out to be its strength!

The recently discovered magnetic arms in the spiral galaxy NGC 6946 (see [3]), where the large-scale magnetic field (unlike the total field) is stronger between the gaseous spiral arms, i.e., where the gas density is lower, directly indicates that the regular magnetic field is not frozen into the ISM and therefore must be maintained against turbulent diffusion.

The complicated magnetic structure in the spiral galaxy M51, where the large-scale magnetic fields in the disc and the halo are almost oppositely directed [7] also requires an explanation more complicated than just a quasi-uniform primordial magnetic field twisted by the galactic differential rotation.

5. Dynamo parameters

Using the parameters of the solar convection zone presented in Sect. 3.1, one obtains $\alpha \simeq l^2 \Omega / h \simeq 2 \times 10^3 \text{ cm s}^{-1}$ (which is close to the convection velocity), and $\eta_t \simeq \frac{1}{3} l v \simeq 10^{12} \text{ cm}^2 \text{ s}^{-1}$. This yields the following crude estimates of the dimensionless numbers that controls the mean-field dynamo action:

$$R_\alpha = \frac{\alpha H}{\eta_t}, \quad R_\omega = \frac{\Delta \Omega H^2}{\eta_t}, \quad D = R_\alpha R_\omega \simeq 4000,$$

where $H = 0.3 R_\odot$ is the thickness of the convection zone. Here R_α and R_ω are the turbulent magnetic Reynolds numbers that characterize the intensities of helical small-scale motions and differential rotation, respectively. Their product, the dynamo number D , quantifies the efficiency of the mean-field dynamo action in systems with strong differential rotation, $|R_\omega| \gg |R_\alpha|$. Here we assume that the solar dynamo acts in the bulk of the convection zone. Dynamo models that explicitly include the tachocline are reviewed in Ref. [51].

For spiral galaxies, assuming a flat rotation curve, $V_0 = r\Omega = \text{const}$, we similarly obtain the following estimates:

$$R_\omega \simeq -3 \frac{V_0}{v} \frac{h^2}{l R_0} \simeq -15, \quad R_\alpha \simeq 3 \frac{V_0}{v} \frac{l}{R_0} \simeq 0.5,$$

where $V_0 = 200 \text{ km s}^{-1}$ is the typical rotational velocity, $v = 10 \text{ km s}^{-1}$, $l = 0.1 \text{ kpc}$, $h = 0.5 \text{ kpc}$ and $R_0 = 10 \text{ kpc}$. Similarly,

$$D = R_\alpha R_\omega \simeq 10 \frac{h^2}{v^2} r \Omega \frac{d\Omega}{dr} \approx -10 \left(\frac{h}{R_0} \right)^2 \left(\frac{V_0}{v} \right)^2 \simeq -10. \quad (5.1)$$

Note that the dynamo number is independent of the turbulent scale and only depends on parameters reasonably well known from observations.

In the case of galaxies, it is useful to define the *local* dynamo parameters R_α and R_ω , as functions of the galactocentric radius r . These are obtained when the r -dependent, local values of the parameters are used instead of the characteristic ones, for example α can be replaced by $l^2(r)\Omega(r)/h(r)$. Then the local dynamo number is given by

$$D_L = \frac{\alpha(r)G(r)h^3(r)}{\eta_t^2(r)} \simeq -10 \left(\frac{\Omega h}{v} \right)^2, \quad (5.2)$$

where $G = rd\Omega(r)/dr$ ($G = -\Omega$ for $\Omega \propto r^{-1}$). The local dynamo number rapidly grows towards the galactic centre (roughly as r^{-1}) mainly due to the increase in Ω . The estimate (5.1) is based on parameter values typical of the Solar vicinity of the Milky Way. In other galaxies and in other parts of our Galaxy, this can be a poor measure of the dynamo activity; unfortunately, this is often forgotten and the single estimate (5.1) is used to represent the whole diverse world of galactic dynamos.

6. Perturbation solutions for mean-field dynamos

6.1. Disc dynamos

In this section we shall develop an approximate solution of the mean-field dynamo equation

$$\frac{\partial \bar{\mathbf{B}}}{\partial t} = \nabla \times (\bar{\mathbf{V}} \times \bar{\mathbf{B}}) + \nabla \times (\alpha \bar{\mathbf{B}}) - \nabla \times \eta_t \nabla \times \bar{\mathbf{B}}. \quad (6.1)$$

It is convenient to introduce cylindrical polar coordinates (r, ϕ, z) with the z -axis parallel to the angular velocity vector $\mathbf{\Omega}$. In a thin disc, all spatial derivatives can be neglected in comparison with those in z , $\partial/\partial z \gg \partial/\partial r, \partial/r\partial\phi$. Then the local dynamo equations, written in the $\alpha\omega$ -approximation, reduce to the following dimensionless form (for $\eta_t = \text{const}$):

$$\frac{\partial \bar{B}_r}{\partial t} = -R_\alpha \frac{\partial}{\partial z} (\alpha \bar{B}_\phi) + \frac{\partial^2 \bar{B}_r}{\partial z^2}, \quad (6.2)$$

$$\frac{\partial \bar{B}_\phi}{\partial t} = R_\omega \bar{B}_r + \frac{\partial^2 \bar{B}_\phi}{\partial z^2}, \quad (6.3)$$

$$\frac{\partial \bar{B}_z}{\partial t} = \frac{\partial^2 \bar{B}_\phi}{\partial z^2}, \quad (6.4)$$

where the units of z and t are h and h^2/η_t , respectively (see [4, 41] for details). Equation for \bar{B}_z splits from the system and Eqs. (6.2) and (6.3) can be solved

separately. The vertical magnetic field in a thin disc is supported through the radial and azimuthal components via their radial derivatives which are neglected in Eqs (6.2)–(6.4). These equations are supplemented with the vacuum boundary conditions

$$\bar{B}_\phi = 0, \quad \bar{B}_r \approx 0, \quad \frac{\partial \bar{B}_z}{\partial z} = 0 \quad \text{at } z = \pm 1, \quad (6.5)$$

and the symmetry conditions at the disc midplane $z = 0$:

$$\frac{\partial \bar{B}_r}{\partial z} = \frac{\partial \bar{B}_\phi}{\partial z} = \bar{B}_z = 0 \quad \text{at } z = 0 \quad (\text{quadrupolar}), \quad (6.6)$$

and

$$\bar{B}_r = \bar{B}_\phi = \frac{\partial \bar{B}_z}{\partial z} = 0 \quad \text{at } z = 0 \quad (\text{dipolar}). \quad (6.7)$$

At the kinematic stage of the dynamo, when the velocity field remains unaffected by the growing magnetic field, we have

$$\bar{\mathbf{B}} = \mathbf{B} \exp(\gamma t).$$

We further rescale the radial magnetic field $\bar{B}_r \rightarrow R_\alpha \bar{B}_r$ to obtain the following boundary value problem involving the dynamo number $D = R_\alpha R_\omega$:

$$\begin{aligned} \gamma \mathcal{B}_r &= -\frac{\partial}{\partial z}(\alpha \mathcal{B}_\phi) + \frac{\partial^2 \mathcal{B}_r}{\partial z^2}, \\ \gamma \mathcal{B}_\phi &= D \mathcal{B}_r + \frac{\partial^2 \mathcal{B}_\phi}{\partial z^2}, \\ \mathcal{B}_r(1) &= \mathcal{B}_\phi(1) = 0, \end{aligned} \quad (6.8)$$

together with (6.6) and (6.7). Thus, we have formulated a one-dimensional boundary value problem with the eigenvalue γ and vectorial eigenfunction $\mathbf{B}(z)$.

6.1.1. Free decay modes

Equations (6.8) can easily be solved in the absence of sources, $\alpha = D = 0$. The resulting solutions, known as *free decay modes*, are doubly degenerate since two distinct eigenfunctions \mathbf{B}_n and \mathbf{B}'_n correspond to each eigenvalue. The pairs of odd modes are given by

$$\begin{aligned} \mathbf{B}_n^{(d)} &= \begin{pmatrix} \sqrt{2} \sin(\pi n z) \\ 0 \end{pmatrix}, \quad \mathbf{B}_n^{(d)'} = \begin{pmatrix} 0 \\ \sqrt{2} \sin(\pi n z) \end{pmatrix}, \\ \gamma_n^{(d)} &= -\pi^2 n^2, \quad n = 1, 2, \dots, \end{aligned}$$

whereas the free decay modes of even parity are

$$\mathcal{B}_n^{(q)} = \begin{pmatrix} \sqrt{2} \cos[\pi(n + \frac{1}{2})z] \\ 0 \end{pmatrix}, \quad \mathcal{B}_n^{(q)'} = \begin{pmatrix} 0 \\ \sqrt{2} \cos[\pi(n + \frac{1}{2})z] \end{pmatrix},$$

$$\gamma_n^{(q)} = -\pi^2(n + \frac{1}{2})^2, \quad n = 0, 1, 2, \dots$$

The eigenfunctions $\mathcal{B}_n = (\mathcal{B}_{rn}, \mathcal{B}_{\phi n})$ have been normalized to have $\int_0^1 \mathcal{B}_n^2 dz = 1$ for both dipolar and quadrupolar cases. The free-decay eigenfunctions form an orthonormal set of basis functions which are used below to develop a perturbation solution for α , $D \neq 0$.

The dipolar mode with $n = 0$ is trivial as the horizontal magnetic field of the corresponding eigenfunction is identically zero, $(\bar{B}_r^{(d)}, \bar{B}_\phi^{(d)}) = 0$ even for $\alpha \neq 0$ and $D \neq 0$. The trivial dipolar solution consists of a uniform vertical magnetic field $B_z = \text{const}$ which is not affected by magnetic diffusion and therefore neither grows nor decays in this approximation.

The lowest quadrupolar mode decays four times as weakly as the lowest non-trivial dipolar one. This fact is closely associated with the property of the lowest quadrupolar mode to be generated preferentially (at a larger growth rate for a given dynamo number) than the dipolar ones. Therefore, large-scale magnetic fields of even parity dominate in spiral galaxies. The preference of even, quadrupolar modes is a specific feature of the disc geometry; in spherical bodies, such as the Sun and the Earth, the dipolar mode is preferred, in agreement with observations.

6.1.2. *The perturbation expansion*

For $|D| \ll 1$, terms containing α and D on the right-hand sides of equations (6.8) can be treated as a small perturbation, and an approximate solution can be obtained by perturbing the free-decay modes obtained for $\alpha = D = 0$. To isolate the perturbation operator, we introduce a new variable $\tilde{\mathcal{B}}_\phi = |D|^{-1/2} \mathcal{B}_\phi$, so that \mathcal{B}_r and $\tilde{\mathcal{B}}_\phi$ are of the same order of magnitude in D . Preserving the original notation for the renormalized azimuthal field component, we rewrite the dynamo equations in the matrix-operator form

$$\gamma \mathcal{B} = (\hat{W} + |D|^{1/2} \hat{V}) \mathcal{B}, \tag{6.9}$$

where

$$\hat{W} = \begin{pmatrix} \frac{d^2}{dz^2} & 0 \\ 0 & \frac{d^2}{dz^2} \end{pmatrix}, \quad \hat{V} \mathcal{B} = \begin{pmatrix} 0 & -\frac{d}{dz}(\alpha \mathcal{B}_r) \\ \mathcal{B}_\phi \text{ sign } D & 0 \end{pmatrix},$$

are the unperturbed (free-decay) and perturbation operators, respectively. The perturbed solution is represented as a superposition of free decay modes. Since each free-decay eigenvalue is doubly degenerate, the perturbation $\epsilon \widehat{V}$ first removes the degeneracy, giving an $O(\epsilon)$ correction to the eigenvalue but and $O(1)$ correction to the eigenfunction (Sect. 33 of [21]). Thus, to the first order, the perturbed leading eigenfunction and eigenvalue have the form

$$\mathcal{B} \approx C_0 \mathcal{B}_0 + C'_0 \mathcal{B}'_0, \quad \gamma \approx \gamma_0 + \epsilon \gamma_1, \tag{6.10}$$

where C_0, C'_0, γ_0 and γ_1 are constants of order unity in ϵ , and the lowest (quadrupolar) free-decay modes \mathcal{B}_0 and \mathcal{B}'_0 are given in Section 6.1.1 [we have dropped the superscript (q) to simplify the notation]. To calculate the expansion coefficients, these forms are substituted into Eq. (6.9); to the zeroth order in ϵ , this yields $\gamma_0 = \lambda_0$. Terms of order ϵ are then isolated, their dot product is taken with \mathcal{B}_0 and then with \mathcal{B}'_0 , and the results are integrated over z from 0 to 1. This brings us to a system of two homogeneous algebraic equations for C_0 and C'_0 :

$$(\gamma_1 - V_{00})C_0 - V_{00'}C'_0 = 0, \quad -V_{0'0}C_0 + (\gamma_1 - V_{0'0'})C'_0 = 0,$$

where $V_{nm} = \int_0^1 \mathcal{B}_n \cdot \widehat{V} \mathcal{B}_m dz$ (and likewise for $V_{n'm'}$, but with \mathcal{B}_n replaced by \mathcal{B}'_n , etc.) are the matrix elements (note that $V_{nn} = V_{n'n'} = 0$). The solvability condition of this system (vanishing of the determinant) yields γ_1 :

$$\gamma_1 = \pm \sqrt{V_{0'0}V_{00'}}, \quad \text{and} \quad C'_0 = \pm C_0 \sqrt{\frac{V_{0'0}}{V_{00'}}}. \tag{6.11}$$

Since we are interested in solutions that decay slower as $|D|$ increases, and then grow when $|D|$ is large enough, we select the upper sign in these relations to have $\gamma_1 > 0$.

A similar solution can be obtained for the dipolar mode, $\mathcal{B} \approx C_1 \mathcal{B}_1^{(d)} + C'_1 \mathcal{B}'_1^{(d)}$.

Having calculated the matrix elements for $\alpha = z$, we obtain

$$\gamma^{(d)} \approx -\pi^2 + \sqrt{-\frac{1}{2}D}, \tag{6.12}$$

$$\gamma^{(q)} \approx -\frac{1}{4}\pi^2 + \sqrt{-\frac{1}{2}D} \tag{6.13}$$

for solutions of dipolar and quadrupolar symmetry, respectively, where we have chosen the sign in front of the square root corresponding to solutions growing for $D < 0$.

The solutions are non-oscillatory, $\text{Im } \gamma = 0$, and they grow if $|D| > |D_c|$ (note that $D, D_c < 0$ in galactic discs), where

$$D_c^{(d)} \approx -2\pi^4 \approx -195, \quad D_c^{(q)} \approx -\frac{1}{8}\pi^4 \approx -12,$$

for the dipolar and quadrupolar modes, respectively. The preference of the quadrupolar modes in a thin disc is now obvious: $|D_c^{(q)}| \ll |D_c^{(d)}|$.

Strictly speaking, this approximate solution should not be extended to estimate D_c because $|D_c|$ is not small. However, such bold extensions of asymptotic solutions often yield useful results. In particular, the above estimates are rather close to those obtained from numerical solutions of the dynamo equations (see below). The reason for that is that the dependence of the growth rate on D has the same form for both $|D| \ll 1$ and $|D| \gg 1$, namely $\gamma = \text{const} + |D|^{1/2}$, where the constant can be neglected for $|D| \gg 1$ [31]. Thus the dependence of γ on D is reasonably approximated by our perturbation solution even for those values of $|D|$ where it is not formally applicable.

Of course, the critical dynamo number depends on the form of $\alpha(z)$. A perturbation solution similar to that given above, but now for $\alpha = \sin \pi z$, gives $D_{\text{cr}}^{(q)} \approx -\frac{1}{4}\pi^3 \approx -8$. Numerical solutions show that the critical dynamo number for the lowest quadrupolar mode lies between approximately -4 and -12 for various forms of $\alpha(z)$. The rather low generation threshold $D_{\text{cr}}^{(q)} \approx -4$ is obtained if the α -effect is concentrated at halfway between the symmetry plane and the surface of the slab, $\alpha = \delta(z - \frac{1}{2}) - \delta(z + \frac{1}{2})$. Smooth distributions of $\alpha(z)$ give higher generation thresholds. For $\alpha = \sin \pi z$, the critical dynamo number obtained numerically is very close to the above approximate value, $D_{\text{cr}}^{(q)} \approx -8$, while $D_{\text{cr}}^{(q)} \approx -11$ for $\alpha = z$ (again in good agreement with the approximate solution). If $\alpha(z)$ is piecewise constant, $\alpha = \theta(z) - \theta(-z)$, $D_{\text{cr}}^{(q)} \approx -6$.

Given the above results for the eigenvalues, the coefficients of the expansion in free-decay modes are related by

$$C'_0 = -\sqrt{2}C_0, \quad \text{for } \alpha = z,$$

for both the quadrupolar and dipolar modes. Restoring the original scaling of the field components ($\mathcal{B}_r \rightarrow R_\alpha \mathcal{B}_r$ and $\mathcal{B}_\phi \rightarrow |D|^{1/2} \mathcal{B}_\phi$), the lowest-order eigenfunctions are obtained as

$$\begin{pmatrix} \mathcal{B}_r \\ \mathcal{B}_\phi \end{pmatrix} \approx C_0 \sqrt{2} \begin{pmatrix} R_\alpha \\ -\sqrt{2}|D|^{1/2} \end{pmatrix} \times \begin{cases} \sin \pi z & (\text{odd modes}), \\ \cos \frac{1}{2}\pi z & (\text{even modes}), \end{cases} \quad (6.14)$$

for $\alpha = z$, where C_0 remains an arbitrary constant. This results in the following estimate of the pitch angle of magnetic lines in the growing (kinematic) solution,

the same for both dipolar and quadrupolar solutions:

$$p_B = \arctan \frac{\bar{B}_r}{\bar{B}_\phi} \approx -\arctan \frac{1}{\sqrt{2}} \sqrt{\frac{R_\alpha}{|R_\omega|}}. \tag{6.15}$$

For $R_\alpha = 1$ and $R_\omega = -20$, this yields $p_B \approx -10^\circ$ in a good agreement with the pitch angles observed in spiral galaxies. For $\alpha = \sin \pi z$, a similar estimate differs insignificantly from the above (prefactor $\sqrt{\pi}/2$ instead of $1/\sqrt{2}$ in the estimate of p_B).

The accuracy of the perturbation solutions developed here is quite satisfactory even for $D \simeq D_c$, so it is worth considering the next approximation in ϵ . In particular, we show in Sect. 6.3 that the radial component, \bar{B}_r , of any growing eigenfunction must change sign near the disc surface (given the vacuum boundary conditions). Since this detail of the eigenfunction appears to be essential for the dynamo action, it is useful to develop a solution that captures this feature. To provide more examples, we present the second-order results for a different choice of the α -coefficient, $\alpha = \sin \pi z$. The second-order quadrupolar solution has the form

$$\mathcal{B} \approx \tilde{\mathcal{B}}_0 + \epsilon \sum_{n=1}^{\infty} (C_n \mathcal{B}_n + C'_n \mathcal{B}'_n),$$

$$\gamma \approx \gamma_0 + \epsilon \gamma_1 + \epsilon^2 \gamma_2,$$

which is useful to compare with Eq. (6.10). Here $\tilde{\mathcal{B}}_0 = C_0 \mathcal{B}_0 + C'_0 \mathcal{B}'_0$ is the properly normalized first-order eigenfunction, $\int_0^1 \tilde{\mathcal{B}}_0^2 dz = 1$:

$$\tilde{\mathcal{B}}_0 = \sqrt{\frac{2}{1 + 4/\pi}} \begin{pmatrix} 1 \\ -2/\sqrt{\pi} \end{pmatrix} \cos \frac{\pi z}{2} \quad \text{for } \alpha = \sin \pi z.$$

As before, these expansions are substituted into the dynamo equations, terms of order ϵ^2 are isolated, dot products with \mathcal{B}_k and \mathcal{B}'_k (with $k \neq 0$) are evaluated and then integrated over z from 0 to 1. This leads to algebraic equations for C_n and C'_n , which yield

$$C_n = \frac{V_{n\tilde{0}}}{\lambda_0 - \lambda_n}, \quad C'_n = \frac{V_{n'\tilde{0}}}{\lambda_0 - \lambda_n},$$

and, from the solvability condition,

$$\gamma_2 = \sum_{n=1}^{\infty} \frac{V_{n\tilde{0}} V_{\tilde{0}n} + V_{n'\tilde{0}} V_{\tilde{0}n'}}{\lambda_0 - \lambda_n},$$

where $V_{n\tilde{0}}$ denotes the matrix element involving \mathcal{B}'_n and $\tilde{\mathcal{B}}'_0$ and similarly for the other matrix elements. Direct calculation yields

$$V_{n\tilde{0}} = \frac{1}{2} \sqrt{\frac{\pi}{1+4/\pi}} \times \begin{cases} 1, & n = 0, \\ 3, & n = 1, \\ 0, & n \neq 0, 1, \end{cases}$$

$$V_{n'\tilde{0}} = -\frac{1}{\sqrt{1+4/\pi}} \times \begin{cases} 1, & n = 0, \\ 0, & n \neq 0, \end{cases}$$

$$V_{\tilde{0}n} = \frac{2}{\sqrt{\pi+4}} \times \begin{cases} 1, & n = 0, \\ 0, & n \neq 0. \end{cases}$$

Thus it can be shown that $\gamma_2 = 0$ for any form of $\alpha(z)$, whereas, for $\alpha = \sin \pi z$,

$$C_n = C'_n = 0 \text{ for } n \neq 1, \quad C_1 = \frac{3}{4\pi^{3/2}\sqrt{1+4/\pi}}.$$

For $D < 0$ and $\alpha = \sin \pi z$, to the second order in $\epsilon = |D|^{1/2}$, the corresponding quadrupolar solution written in terms of the physical variables follows as

$$\mathcal{B}_r = R_\alpha C_0 \left(\cos \frac{\pi z}{2} + \frac{3}{4\pi^{3/2}} \sqrt{-D} \cos \frac{3\pi z}{2} \right) + O(D), \tag{6.16}$$

$$\mathcal{B}_\phi = -2C_0 \sqrt{-\frac{D}{\pi}} \cos \frac{3\pi z}{2} + O(D), \tag{6.17}$$

$$\gamma = -\frac{\pi^2}{4} + \frac{1}{2} \sqrt{-\pi D} + O(|D|^{3/2}). \tag{6.18}$$

This solution is remarkably accurate even for D close to the critical value; in particular, it yields $D_c \approx -7.8$, as compared with the numerically obtained value of -8 , and the eigenfunction shown in Fig. 2 for $|D| \lesssim 20$ is practically indistinguishable from the numerical solution.

6.2. Spherical shell dynamos

Perturbation solutions similar to those developed in Sect. 6.1 can be obtained for other dynamo systems. Here we illustrate the techniques using Parker's model of the mean-field dynamo in a thin spherical shell, where the dominant modes are oscillatory, and the unperturbed state is not degenerate. In terms of the (scaled) azimuthal components of the vector potential, $\bar{A}_\phi = \mathcal{A} \exp \gamma t$, and magnetic

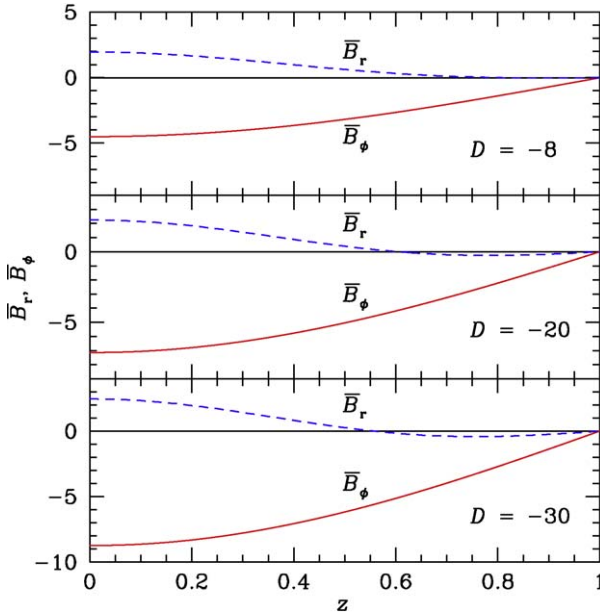


Fig. 2. The approximate eigenfunctions B_r (dashed) and B_ϕ (solid) for $\alpha = \sin \pi z$ from Eqs (6.16)–(6.17) for $D = -8, -20, -30$ (with $D_c \approx -8$), $C_0 = 1$ and $R_\alpha = 1$.

field, $\bar{B}_\phi = \mathcal{B} \exp \gamma t$, the $\alpha\omega$ -dynamo equations in a thin shell can be written as [28]

$$\gamma \mathcal{A} = \alpha(\theta) \mathcal{B} + \frac{\partial^2 \mathcal{A}}{\partial \theta^2}, \tag{6.19}$$

$$\gamma \mathcal{B} = -D \cos \theta \frac{\partial \mathcal{A}}{\partial \theta} + \frac{\partial^2 \mathcal{B}}{\partial \theta^2}, \tag{6.20}$$

where θ is the latitude, $D (< 0)$ is the dynamo number, the angular velocity is assumed to depend on the spherical radius alone, and we consider axially symmetric solutions. The simplest model assumes that $\alpha = \sin \theta$, and we shall be adopting this form in what follows.

The boundary conditions at the equator,

$$\mathcal{B}(0) = 0, \quad \frac{\partial \mathcal{A}}{\partial \theta}(0) = 0,$$

isolate dipolar modes as appropriate for the Sun. Obviously,

$$\mathcal{B}(\pi/2) = 0,$$

but the boundary condition for \mathcal{A} at the pole is more difficult to establish. We are interested here in modelling the main branch of the dynamo wave that propagates from mid-latitudes towards the equator. It is launched away from the pole, at about $\theta = 30^\circ$, and there is another branch that propagates from the mid-latitudes to the pole. Thus, the solution we are interested in does not reach the pole, and the boundary condition for it could be posed at some intermediate latitude not known in advance. To simplify the model, we still pose it at $\theta = \pi/2$ but select it as to obtain a desired migratory wave solution. Our experimentation with different forms of this boundary condition suggests that the perturbation solution is oscillatory for

$$\left(\frac{\partial \mathcal{A}}{\partial \theta} + i\xi \mathcal{A} \right) \Big|_{\theta=\pi/2} = 0,$$

where ξ is an arbitrary real constant.

As in Sect. 6.1, we renormalize $\mathcal{B} = \mathcal{B}'\sqrt{|D|}$ to recast Eqs (6.19) and (6.20) in the form (we drop prime at \mathcal{B}')

$$\gamma \begin{pmatrix} \mathcal{A} \\ \mathcal{B} \end{pmatrix} = \widehat{W} \begin{pmatrix} \mathcal{A} \\ \mathcal{B} \end{pmatrix} + \epsilon \widehat{V} \begin{pmatrix} \mathcal{A} \\ \mathcal{B} \end{pmatrix},$$

where

$$\epsilon = |D|^{1/2}, \quad \widehat{W} = \begin{pmatrix} \frac{\partial^2}{\partial \theta^2} & 0 \\ 0 & \frac{\partial^2}{\partial \theta^2} \end{pmatrix}, \quad \widehat{V} = \begin{pmatrix} 0 & \alpha \\ \cos \theta \frac{\partial}{\partial \theta} & 0 \end{pmatrix}.$$

For $\epsilon = 0$, Eqs. (6.19) and (6.20) decouple and the free-decay modes can easily be found. One of them is given by

$$\begin{pmatrix} \mathcal{A}_m \\ \mathcal{B}_m \end{pmatrix} = \begin{pmatrix} 0 \\ 2\pi^{-1/2} \sin 2m\theta \end{pmatrix}, \quad \lambda'_m = -4m^2, \quad m = 0, 1, \dots,$$

and the other is

$$\begin{pmatrix} \mathcal{A}_n \\ \mathcal{B}_n \end{pmatrix} = C \begin{pmatrix} \cos(\sqrt{-\lambda_n}\theta) \\ 0 \end{pmatrix}, \quad \sqrt{-\lambda_n} \tan(\pi\sqrt{-\lambda_n}/2) = i\xi,$$

where C is the normalization constant. The transcendental equation for λ_n can be solved in approximate manner for $|\xi| \gg 1$ with the *ansatz* $\sqrt{-\lambda_n} = 1 - x$ with $|x| \ll 1$ to yield $\sqrt{-\lambda_n} \approx 1 + 2i/(\pi\xi) + 4n$, or

$$\lambda_n \approx -(1 + 4n)^2 - \frac{4i}{\pi\xi}(1 + 4n), \quad n = 0, 1, \dots$$

The normalization $\int_0^{\pi/2} |\mathcal{A}_n|^2 d\theta = 1$ then yields $C \approx 2/\sqrt{\pi}$.

To lowest order, the perturbed solution that contains both azimuthal and meridional components has the form

$$\begin{pmatrix} \mathcal{A} \\ \mathcal{B} \end{pmatrix} = C_0 \begin{pmatrix} \mathcal{A}_0 \\ 0 \end{pmatrix} + C_1 \begin{pmatrix} 0 \\ \mathcal{B}_1 \end{pmatrix},$$

which yields, for the leading eigenfunction,

$$\gamma \approx \lambda_0 - \epsilon^2 \frac{V_{01} V_{10}}{(\lambda_0 - \lambda'_1)^2},$$

where

$$V_{01} \approx \frac{1}{2}, \quad V_{10} \approx -\frac{2}{\pi} \left(1 + \frac{2i}{\pi \xi} \right).$$

Thus,

$$\gamma \approx -1 - \frac{4i}{\pi \xi} - \frac{1}{9\pi} D,$$

so that the critical value of the dynamo number, corresponding to $\text{Re } \gamma = 0$, is $D_c \approx -9\pi$. The cycle frequency of this solution, $\omega = 4/(\pi \xi)$, is controlled by the magnitude of ξ . In terms of dimensional variables, to obtain the cycle period $T = 22$ yr, we need $\xi = 2T \eta_t / (\pi H)^2 \approx 0.3$, where $\eta_t = 10^{12} \text{ cm}^2 \text{ s}^{-1}$ is the turbulent magnetic diffusivity in the Solar convection zone and $H = 0.2R_\odot$ is the thickness of the convection zone. We note that the value of ξ required to fit the period of the dynamo cycle is not much larger than one as assumed when deriving the above solution.

6.3. Diffusion in mean-field dynamos

Integrating the thin-disc dynamo equations (6.2) and (6.3), written in the dimensional form, over the interval $0 < z < h$ for a smooth function $\alpha(z)$ gives:

$$\frac{\partial}{\partial t} \int_0^h \bar{B}_r \, dz = \eta_t \frac{\partial \bar{B}_r}{\partial z}(h), \tag{6.21}$$

$$\frac{\partial}{\partial t} \int_0^h \bar{B}_\phi \, dz = G \int_0^h \bar{B}_r \, dz + \eta_t \frac{\partial \bar{B}_\phi}{\partial z}(h), \tag{6.22}$$

where $G = r \, d\Omega/dr$ and we have used the quadrupolar symmetry conditions (6.6). It is notable that α does not enter the integrated equations because $\alpha(0) = 0$ and $\bar{B}_\phi(1) = 0$.

The integral form of the dynamo equations (6.21) and (6.22) highlights the role of magnetic diffusivity in the dynamo mechanism. It would seem at first

glance that magnetic diffusion can be neglected for the growing solutions. However, setting $\eta_t = 0$ in (6.21) (more precisely, supposing that both the turbulent and Ohmic diffusivities vanish), results in $\int_0^h \bar{B}_r dz = \text{const}$, and then (6.22) shows that $\int_0^h \bar{B}_\phi dz$ can grow only linearly in time. In other words, the solution cannot grow exponentially if $\eta_t = 0$ (and thus the dynamo action is impossible). In the more general case where η_t varies with z , the dynamo action requires that $\eta_t(h) \neq 0$.

Consider a function $\bar{B}_\phi(z)$ that has no zeros and, say, $\bar{B}_\phi > 0$ for $0 < z < h$. It is expected that such a function corresponds to the lowest excited mode. Since $\bar{B}_\phi(h) = 0$, this implies that

$$\frac{\partial \bar{B}_\phi}{\partial z}(h) < 0.$$

Then Eqs (6.21) and (6.22) imply, for $G < 0$, that any growing even solution must satisfy the following inequalities:

$$\int_0^h \bar{B}_r dz < 0, \quad \eta_t \frac{\partial \bar{B}_r}{\partial z}(h) < 0. \tag{6.23}$$

Hence, the radial component of a growing magnetic field must change its sign near the disc surface.

The second inequality of (6.23) shows that the dynamo action requires non-vanishing flux of the radial magnetic field across the disc surface. The role of diffusion can also be seen directly from the dynamo equations. For definiteness, assume again that $G < 0$, $\bar{B}_\phi > 0$, and, near the symmetry plane, $\bar{B}_r < 0$. The α -effect generates, via the term $-\partial(\alpha \bar{B}_\phi)/\partial z$, a positive radial field, i.e., a radial field opposite to that of the growing solution near the symmetry plane. The positive \bar{B}_r near the surface produces, through differential rotation $-|G| \bar{B}_r$, a negative contribution to $\partial \bar{B}_\phi / \partial t$, which can be compensated only by the viscous term, $\eta_t \partial^2 \bar{B}_\phi / \partial z^2$. In order to provide such a compensation, the latter term must be positive near the disc surface, i.e., the field must be transported outwards. It also becomes clear that, in addition to conditions (6.23), $\bar{B}_\phi(z)$ must have an inflection point at somewhat smaller z than the zero of \bar{B}_r .

On the other hand, the diffusivity should not be excessively large, otherwise the field would rapidly decay within the main part of the disc and would be carried out toward the disc surface.

The discussion above referred to the growing solutions. In the stationary case ($\partial/\partial t = 0$), we have

$$\eta_t \frac{\partial \bar{B}_r}{\partial z} = 0, \quad \eta_t \frac{\partial^2 \bar{B}_\phi}{\partial z^2} = 0 \quad \text{at } z = h,$$

i.e., both horizontal (parallel to the disc midplane) field components have fixed (and opposite) signs within the disc.

The forms of $\bar{B}_r(z)$ and \bar{B}_ϕ shown in Fig. 2 for a large, moderate and critical value of $|D|$ illustrate these properties of the growing and marginal solutions of the dynamo equations.

7. Turbulent magnetic fields in galaxies and galaxy clusters

7.1. The fluctuation dynamo

The evolution of a magnetic field embedded into a flow of conducting fluid is controlled by the magnetic Reynolds number,

$$R_m = \frac{v_0 l_0}{\eta},$$

where v_0 and l_0 are the representative velocity and scale in the flow and η is the turbulent magnetic diffusivity. In turbulent flows without any mean velocity, it is convenient to choose l_0 and v_0 as the integral scale and velocity at that scale (these quantities were denoted l and v above; in this section, we label them with subscript zero). The larger is R_m , the better is the magnetic flux freezing approximation, i.e., the better magnetic lines follow the fluid particles.

The generation of a random magnetic field by a random flow, called the *fluctuation dynamo*, is a result of a random stretching of magnetic field by the local velocity shear (see reviews in [9, 38, 56]).¹ This type of dynamo does not require any mean flow, rotation or helicity, but only needs a random flow. Magnetic field produced by the fluctuation dynamo is purely random, i.e., its mean value vanishes. The root-mean-square magnetic field (or, equivalently, mean magnetic energy density) can grow under a fairly weak condition $R_m > R_{mc} \simeq 30\text{--}100$ (where the variation within the range depends on the form of the velocity correlation function).

A turbulent flow consists of a broad spectrum of motions, with v_l the velocity at a scale l . The e -folding time for the magnetic field is roughly equal to the 'eddy turnover time' l/v_l . In the Kolmogorov turbulence, where $v_l \propto l^{1/3}$, the e -folding time is shorter at smaller scales, $l/v_l \propto l^{2/3}$, and so smaller eddies amplify the field faster. As a result, most of the magnetic energy produced by the fluctuation dynamo at its *kinematic* stage (i.e., the stage of exponential growth) is at small scales comparable to the magnetic dissipation scale of order $R_m^{-1/2}$. At the kinematic stage, the root-mean-square magnetic field grows as $b \propto \exp \sigma t$

¹This type of dynamo is also called the *small-scale dynamo*, with reference to the fact that the scale of the magnetic field does not exceed l_0 .

with $\sigma \simeq \frac{2}{3}(v_0/l_0) \ln(R_m/R_{mc})$ for $R_m \gg 1$ [30]; numerical results show that this form is quite accurate for R_m of the order of or even smaller than R_{mc} [55].

Since $\eta \ll \nu$ in rarefied astrophysical plasmas, where ν is the kinematic viscosity (see, e.g., [9]), we have $R_m \gg Re$, where $Re = v_0 l_0 / \nu$ is the kinematic Reynolds number. Therefore, $R_m > R_{mc}$ if Re is large enough. Turbulent systems necessarily have large Re , and random motions in galaxies and galaxy clusters will be a fluctuation dynamo for any Reynolds number which is large enough to make them turbulent.

The fluctuation dynamo is sensitive to the value of the magnetic Prandtl number, $Pr_m = \nu/\eta = R_m/Re$ [36]. For $Pr_m > 1$ (intergalactic and interstellar gas) magnetic spectrum extends to smaller scales than the kinetic energy spectrum, whereas for $Pr_m < 1$ the Ohmic dissipation scale is larger than the viscous scale. The dynamo action for $Pr_m \geq 1$ has been demonstrated convincingly with various analytical and numerical models. For $Pr_m < 1$, the dynamo action is also possible but requires larger values of R_m than for $Pr_m > 1$ [19]. The situation at very small values of Pr_m remains unclear, but asymptotic results obtained for a δ -correlated velocity field suggest that $R_{mc} \rightarrow 400$ for $Pr_m \rightarrow 0$ [30].

In the kinematic regime, the fluctuation dynamo produces intermittent magnetic field: the size of the magnetic structures is, in at least one dimension, as small as the resistive scale

$$l_\eta = l_0 R_m^{-1/2} \tag{7.1}$$

in a single-scale flow [56]. We note that magnetic field at the small Ohmic diffusion scale l_η is produced by the shear of the flow at a larger scale l_0 . In a turbulent flow, where a broad spectrum of motions is present, flow at each scale l would produce magnetic structures at scales down to the corresponding Ohmic scale. In the kinematic regime this would correspond to a set of eigenfunctions, each with a distinct growth rate v_l/l . The fastest growing eigenfunction is due to stretching by the smallest eddies with scale l such that $R_m(l) > R_{mc}$, where $R_m(l) = R_m(l/l_0)^{3/4}$ for the Kolmogorov spectrum. These are the viscous scale eddies, with $l = l_\nu = l_0 Re^{-3/4}$, provided $R_m/Re > R_{mc}$. However in the nonlinear regime, when the fastest growing mode saturates, magnetic modes of larger scales still can grow. Since most of the kinetic energy is contained at the scale l_0 , the dominant magnetic scale could still be determined by dynamo action due to eddies of scale l_0 and, especially, by the subtle details of the dynamo saturation. An estimate of the scale of magnetic structures similar to (7.1) but now with allowance for a broad flow spectrum can be obtained from the balance of the stretching and dissipation terms in the induction equation. With l_B the scale of magnetic field, this balance yields $|(\mathbf{B} \cdot \nabla)\mathbf{v}| \simeq |\eta \nabla^2 \mathbf{B}|$, or $l_B v(l_B) \simeq \eta$ provided $l_B > l_\nu$ (this inequality may hold also for $Pr_m > 1$ in the nonlinear state). In a

flow with kinetic energy spectrum

$$E(k) \propto k^{-s} \tag{7.2}$$

(with $s = 5/3$ corresponding to the Kolmogorov spectrum), we have $v^2(l) = k^{-1} E(k)$, so that $v(l) = v_0(l/l_0)^{(s-1)/2}$. This leads to

$$l_B \simeq l_0 R_m^{-2/(s+1)}. \tag{7.3}$$

Nonlinear effects can modify the resulting magnetic structures, although it is as yet not clear in what way [9, 38]). A simple model of Subramanian [49] suggests that the smallest scale of the magnetic structures will be renormalized in the saturated state to become

$$l_B \simeq l_0 R_{mc}^{-2/(s+1)}, \tag{7.4}$$

instead of the resistive scale l_η .

7.2. Shapefinders

Magnetic field produced by a (kinematic) fluctuation dynamo [55] is illustrated in Fig. 3. The velocity field used in this model has a well defined and controllable power-law range (7.2) and allows us to test the theoretical predictions, such as (7.1), (7.3) and (7.4). The structures generated by the fluctuation dynamo are

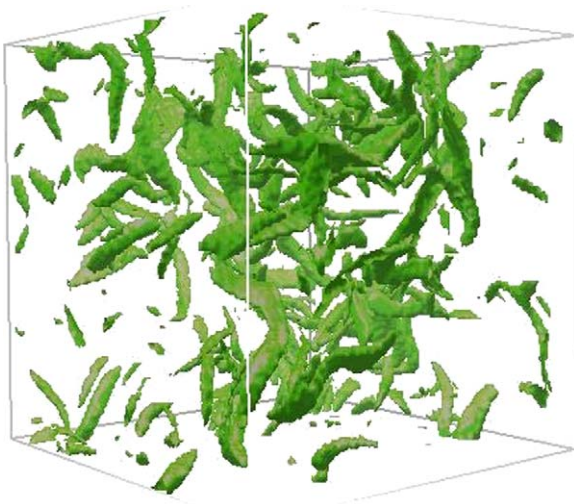


Fig. 3. Isosurfaces $B^2 = 3\langle B^2 \rangle$ from a kinematic fluctuation dynamo model [55].

evidently elongated; they were variously described as magnetic filaments, sheets or ribbons from the visual inspection of magnetic isosurfaces and application of heuristic morphology indicators. A mathematically justifiable approach to the morphology of random magnetic structures based on the *Minkowski functionals* was employed in Ref. [55]. This tool has previously been applied to galaxy distribution and cosmological structure formation [25, 33, 40].

As an example, consider statistical properties of the isosurfaces $B^2 = \text{const}$ similar to those shown in Fig. 3. The topological and geometrical properties of structures in three dimensions can be fully quantified using the four Minkowski functionals [25]:

$$\begin{aligned} V_0 &= \iiint dV, & V_1 &= \frac{1}{6} \iint dS, \\ V_2 &= \frac{1}{6\pi} \iint (\kappa_1 + \kappa_2) dS, & V_3 &= \frac{1}{4\pi} \iint \kappa_1 \kappa_2 dS, \end{aligned} \tag{7.5}$$

where integration is over the volume and surface of the structures, respectively, and κ_1 and κ_2 are the principal curvatures of the surface. V_0 is the total volume enclosed by the structures, V_1 is their surface area, V_2 is the integral mean curvature of their surfaces, and V_3 is the integral Gaussian curvature (related to the Euler characteristic). A simple method to compute the Minkowski functionals for structures given on a grid is based on the intersection formula of Crofton [39]:

$$\begin{aligned} V_0 &= n_3, & V_1 &= \frac{2(n_2 - 3n_3)}{9N}, \\ V_2 &= \frac{2(n_1 - 2n_2 + 3n_3)}{9N^2}, & V_3 &= \frac{n_0 - n_1 + n_2 - n_3}{N^3}, \end{aligned}$$

where n_0 is the number of grid vertices within the structures, n_1 is the number of complete edges, n_2 is the number of complete grid cell faces, n_3 is the number of complete grid cubes within the structures, and N is the total number of grid points in the domain.

The Minkowski functionals can be used to calculate the typical thickness, width and length of the structures, as $T = V_0/2V_1$, $W = 2V_1/\pi V_2$, and $L = 3V_2/4V_3$, respectively. Then, useful dimensionless measures of ‘planarity’ P , and ‘filamentarity’ F can be defined as [33]

$$P = \frac{W - T}{W + T}, \quad F = \frac{L - W}{L + W}.$$

In idealized cases and for convex surfaces, values of P and F lie between zero and unity. For example, an infinitely thin pancake has $(P, F) = (1, 0)$, a perfect filament has $(P, F) = (0, 1)$, whereas $(P, F) = (0, 0)$ for a sphere. We

note that the unit cube has $T = 3/4$, $W = 2/\pi$, $L = 1/2$, thus we do not always have $T < W < L$. Deviations from this ordering are relatively rare for random fields studied here, yet to avoid confusion we introduce the notation $l_1 = \min(T, W, L)$, $l_2 = \text{med}(T, W, L)$ and $l_3 = \max(T, W, L)$.

As discussed in Ref. [55], the filamentarity of magnetic structures produced by the fluctuation dynamo, F , increases faster than P with R_m , so the structures are better described as filaments, especially at the larger values of R_m —see Eq. (7.6) below. Remarkably, velocity field structures of that model are not filamentary since the velocity field at small scales is nearly isotropic. Correspondingly, the isosurfaces of v^2 have negligible planarity and filamentarity. The isosurface of vorticity Ω with $\Omega^2 = 4\langle\Omega^2\rangle$ has $(P, F) = (0.18, 0.11)$; similarly the isosurface of the total strain ($S^2 = S_{ij}S_{ij}$) with $S^2 = 4.5\langle S^2\rangle$ has $(P, F) = (0.11, 0.16)$. Thus, the morphology of the magnetic field is controlled by the nature of the dynamo action rather than by immediate features of the velocity field. The isosurfaces of the electric current density $\mathbf{J} = \nabla \times \mathbf{B}$ are ribbon-like, with $(P, F) = (0.57, 0.82)$ at a level $J^2 = 4\langle J^2\rangle$ for $R_m \approx 1500$.

Using the Minkowski functionals, we can also reliably measure the characteristic length scales of magnetic structures and explore their scalings with R_m and s . In the left panel of Fig. 4, we show l_1 versus R_m at two instants in time for a flow with $s = 5/3$. Whilst the behavior for $R_m \ll R_{mc}$ shows variations in time, we observe for $R_m \gtrsim 200$ a time-independent scaling of the thickness of magnetic structures: $l_1 \propto R_m^{-3/4}$ in agreement with Eq. (7.3).

The right panel of Fig. 4 shows variation with R_m of the characteristic width l_2 and length l_3 of the magnetic structures. For $R_m \gtrsim 200$ we observe another

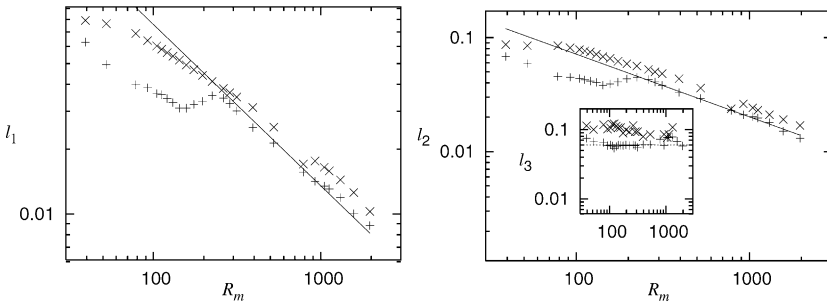


Fig. 4. Average values of the thickness l_1 (left panel), width l_2 (main frame of the right panel) and length l_3 (inset) of the magnetic isosurfaces versus R_m at two instants in time, from the fluctuation dynamo model of Ref. [55]. Data marked ‘x’ (‘+’) are results attained when the smallest eddies have made 25 (50) revolutions. The solid straight line has a slope of $-3/4$ in the left panel and -0.55 in the right one. The unit length is the size of the computational box. The data were obtained by averaging over eight isosurface families $B^2 = q\langle B^2\rangle$ with $q = 1.5, 2, 2.5, \dots, 5$.

time-independent scaling, $l_2 \propto R_m^{-0.55}$. This distinct behavior of the width of magnetic structures has not been obtained in earlier analytical or numerical studies of the fluctuation dynamo. The simultaneous decrease of l_2 and l_1 , coupled with the approximately R_m -independent behavior of l_3 (inset in the right panel of Fig. 4) supports the notion that the magnetic structures become filamentary as R_m increases. Indeed, using $l_1 \simeq 2.4R_m^{-0.75}$, $l_2 \simeq 0.9R_m^{-0.55}$ and $l_3 \simeq 0.05R_m^0$ in the definitions of P and F , we obtain, for $s = 5/3$,

$$P \simeq 1 - 2\left[1 + \frac{3}{8}R_m^{0.2}\right]^{-1}, \quad F \sim 1 - 2\left[1 + \frac{1}{18}R_m^{0.55}\right]^{-1}, \quad (7.6)$$

so that $F > P$ for $R_m \gtrsim 200$.

To investigate how the scaling laws identified via the Minkowski functionals compare with those inferred from other measures, we calculated the inverse ‘integral scale’ of the magnetic field, $2\pi/l_I = \int kM(k) dk / \int M(k) dk$, where $M(k)$ is the magnetic spectral density defined similarly to $E(k)$. We found that l_I follows a scaling of $R_m^{-0.42}$, which understandably differs from the scalings of l_1 , l_2 and l_3 . The scale l_I is a poor measure of the dimension of anisotropic magnetic structures such as filaments. We note that the above scaling of l_I is maintained for *all* subcritical and supercritical values of R_m , unlike the results illustrated in Fig. 4 which display well-defined, time-independent scalings only for $R_m \gtrsim 200$. The scaling (7.3) emerges for $s = 5/3, 2, 3$ [55]. On the contrary, $l_2 \sim R_m^{-0.55}$ independently of s . Asymptotic solutions [30] suggest that the small-scale dynamo (with $\text{Pr}_m < 1$) is only possible for $s > 3/2$. The results of Ref. [55] show that, for high effective Pr_m , the dynamo action is possible for $s = 1$ as well, although a scaling different from Eq. (7.3) is exhibited. It appears that the nature of the

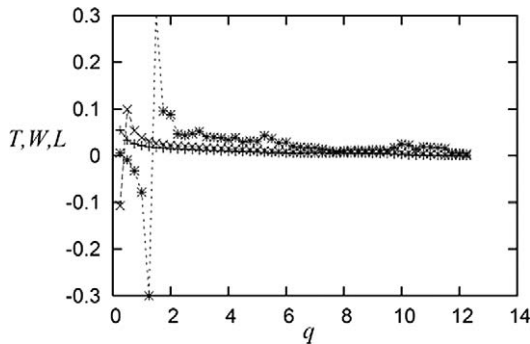


Fig. 5. T , W and L (lines marked with +, \times and *, respectively) as a function of the isosurface level, $B = q\langle B^2 \rangle^{1/2}$ for a dynamo-generated field ($R_m = 1300$). Calculations for $q < 1$ generate anomalous results, whereas the range $1.5 < q < 5$ appears to be acceptable for generating the averages as we discuss in the text.

asymptotic solution, rather than the possibility of a dynamo, is different at $s = 1$ from that at $s > 3/2$.

7.3. Turbulence in galaxy clusters: three evolutionary stages

7.3.1. The epoch of major mergers

Theories of hierarchical structure formation suggest that clusters of galaxies have been assembled relatively recently. N -body simulations indicate that the clusters form at the intersection of dark matter filaments in the large-scale structure, and result from both major mergers of objects of comparable mass (of order $10^{15} M_{\odot}$) and the accretion of smaller clumps onto massive protoclusters. It is likely that intense random vortical flows, if not turbulence, are produced in the merger events. Their plausible properties are summarized in Table 2 (see Ref. [50] for details). The structure of magnetic field at this stage is illustrated in the left-hand panel of Fig. 6. What is shown is the statistically steady state of magnetic field produced by dynamo action in turbulent flow with the Reynolds number about 400 and the magnetic Prandtl number equal to unity. Similar magnetic structure plausibly occur in the turbulent wakes of subclusters and galaxies as well.

It is not quite clear whether random flows driven during major merger events and at later stages of evolution will develop into turbulence. The nature of the flow depends on the value the Reynolds number which is difficult to estimate reliably for the collisionless, magnetized plasma of the intracluster space where plasma instabilities can be responsible for anomalous viscosity and resistivity [37]. The problem is further complicated by the possibility of dynamo action, since the magnetic field can affect both viscosity and magnetic diffusivity. This

Table 2

Summary of turbulence and magnetic field parameters at various stages of cluster evolution: duration of the stage (the last two stages represent steady states), the root-mean-square velocity v_0 and scale l_0 of turbulence and eddy turnover time $t_0 = l_0/v_0$ (for the decaying turbulence, values for the middle of the decay stage are given, 2 Gyr after its start), the equipartition magnetic field $B_{\text{eq}} = (4\pi\rho v_0^2)^{1/2}$ with ρ the gas density (i.e., maximum field strength within a turbulent cell), thickness of magnetic filaments and sheets l_B for the statistically steady state of the dynamo, the root-mean-square magnetic field within a turbulent cell B_{rms} , and finally the standard deviation of the Faraday rotation measure σ_{RM} (calculated for the volume filling turbulence along path length of 750 kpc through the central parts of a cluster in the first two lines, and assuming one transverse wake along the line of sight in the last two lines). A subcluster mass of $3 \times 10^{13} M_{\odot}$ has been assumed

Evolution stage	Length (Gyr)	v_0 (km/s)	l_0 (kpc)	t_0 (Gyr)	B_{eq} (μG)	l_B (kpc)	B_{rms} (μG)	σ_{RM} (rad/m ²)
Major mergers	4	300	150	0.5	4	25	1.8	200
Decaying turbulence	5	130	260	2.0	2	44	0.8	120
Subcluster wakes		260	200	0.8	4	34	1.6	110
Galactic wakes		300	8	0.03	4	1.4	1.6	5

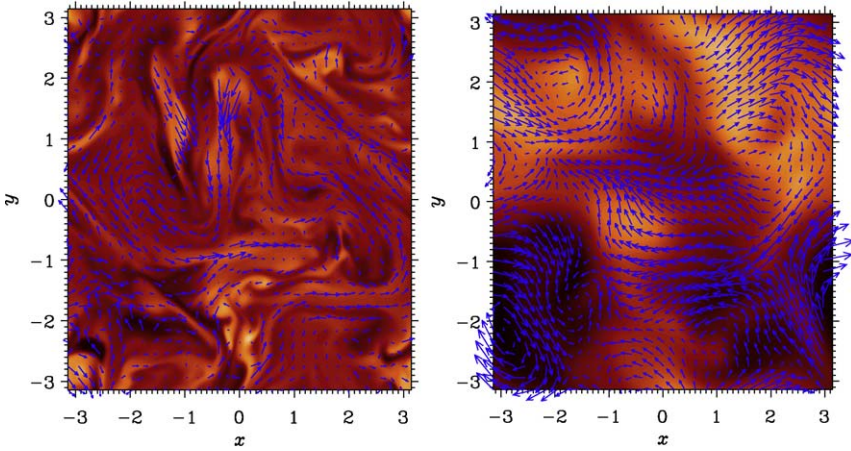


Fig. 6. Snapshots of magnetic field in a cross-section through the middle of the computational domain in a numerical simulation of turbulence driven by an imposed random force and its dynamo action [50]. The left-hand panel shows a statistically steady state at a time $t/t_{0i} = 0.30$ whereas the right-hand panel illustrates magnetic field structures in turbulence at a late stage of decay, $t/t_{0i} \approx 60$. Here t_{0i} is the eddy turnover time before the start of the turbulence decay (given in Table 2). The dimensionless energy injection scale in these simulations is about 4 (with the domain size of 2π), so each frame contains a few turbulent cells. The strongest magnetic field within the frame is close to the equipartition value with respect to the turbulent energy. The magnitude of the field component perpendicular to the plane of the figure is shown color coded (in shades of grey) with black corresponding to field pointing into the figure plane, and lighter shades, to field pointing out of the plane. The field in the plane of the figure is shown with vectors whose length is proportional to the field strength.

may lead to the growth of the magnetic diffusivity and reduction of viscosity as the magnetic field is being amplified by the dynamo, so that the magnetic Prandtl number tends to unity.

7.3.2. Decaying turbulence

Random flows produced by major mergers decay after the end of the merger event. Unlike a laminar flow that decays exponentially in time due to viscosity, turbulent kinetic energy decays slower, as a power law [14, 22]. The reason for this is that kinetic energy mainly decays at small scales, to where it is constantly supplied by the turbulent cascade. As a result, the energy decay rate depends nonlinearly on the energy itself, which makes the decay a power law in time. Our simulations confirm that the power-law decay occurs even for the Reynolds number as small as $\text{Re} \approx 100$ [50]. At this stage of evolution, the turbulent scale l_0 grows with time, whereas turbulent energy density E reduces, together with

the turbulent speed v_0 , typically as

$$E \simeq \frac{1}{2}v_0^2 \propto (t/t_{0i})^{-6/5}, \quad l_0 \propto (t/t_{0i})^{2/5} \quad \text{for } t/t_{0i} \gg 1,$$

where subscript 'i' refers to the start of the evolution, t_{0i} is a certain dynamical time scale, which can be identified with the initial turnover time of the energy-containing eddies, $t_{0i} = l_{0i}/v_{0i}$, subscript '0' refers to the energy-range (correlation) scale of the motion. The structure of magnetic field in the decaying flow is shown in the right-hand panel of Fig. 6, and parameters of the flow and magnetic field are shown in the second line of Table 2.

7.3.3. Turbulent wakes of subclusters and galaxies

At the final stage of the evolution, when the cluster enters a steady state, turbulence is maintained only in the wakes of galaxies and smaller mass clumps that continue to accrete onto the cluster. The wakes become weaker as the gas within the clumps or galaxies is stripped by the ram pressure of intracluster gas. The radius of a wake at its head is close to the radius within which gas of the mass clump or galaxy remains intact. We estimate the stripping radius as $R_0 \simeq 100$ kpc for clumps of a mass $10^{13} M_\odot$ (which fall into a cluster every 3 Gyr) and $R_0 = 3\text{--}5$ kpc for massive elliptical galaxies. If the flow within the wake becomes turbulent (so that it can be described in terms of Prandtl's theory of turbulent wakes [22]), the wake length X is controlled by the magnitude of the Reynolds number via

$$X/R_0 \simeq (\text{Re}_i/\text{Re}_c)^3,$$

where $\text{Re}_c \approx 400$ [52] is the marginal Reynolds number with respect to the onset of turbulence. This value of Re_c was obtained for a flow around a solid sphere; Re_c for gas spheres is not known. The strong dependence of the wake parameters on the Reynolds number makes the estimates somewhat uncertain. On the other hand, it implies that galactic wakes can be very sensitive to the detailed parameters of the galactic motion and intergalactic gas, so that clusters with very similar parameters can have vastly different wake structures.

The area covering and volume filling factors, f_S and f_V , respectively, of $N = 5$ wakes, produced by $10^{13} M_\odot$ subclusters, within the virial radius $r \approx 3$ Mpc, are estimated as

$$f_S \simeq 0.15 \frac{N}{5} \left(\frac{R_0}{100 \text{ kpc}} \right)^6 \left(\frac{\text{Re}_c}{400} \right)^{-4} \left(\frac{\tilde{\lambda}}{1 \text{ kpc}} \right)^{-4},$$

$$f_V \simeq 0.02 \frac{N}{5} \left(\frac{R_0}{100 \text{ kpc}} \right)^8 \left(\frac{\text{Re}_c}{400} \right)^{-5} \left(\frac{\tilde{\lambda}}{1 \text{ kpc}} \right)^{-5},$$

where $N \approx 5$ is consistent with models of hierarchical structure formation, and $\tilde{\lambda}$ is an effective mean free path in the intracluster gas (its introduction is an attempt to allow for our insufficient understanding of viscosity mechanisms). The covering and filling factors strongly depend on $\tilde{\lambda}$ and Re_c . Furthermore, both f_S and f_V depend on high powers of another poorly known parameter, the stripping radius R_0 . Hence, as noted above, properties of the subcluster wakes can be rather different in apparently similar clusters. In addition, numerical simulations of turbulent wakes should be treated with caution as otherwise reasonable approximations, numerical resolution, and numerical viscosities can strongly affect the results. On the other hand, it is plausible that $f_S = O(1)$ but $f_V \ll 1$, so that a typical line of sight through the cluster intersects at least one turbulent region (where our estimate of the r.m.s. turbulent speed is $200\text{--}300 \text{ km s}^{-1}$) despite the fact that turbulence occurs only in a small fraction of the cluster volume. A possible signature of such spatially intermittent turbulence could be a specific shape of spectral lines, with a narrow core, produced in quiescent regions, accompanied by nonthermally broadened wings.

The area covering factor of galactic wakes within the gas core radius, 180 kpc, is unity if

$$X/R_0 \simeq 30\text{--}15, \quad X \simeq 100\text{--}70 \text{ kpc}, \quad (7.7)$$

and the volume filling factor of such wakes is $f_V \simeq 0.07$. The length of galactic wakes required to cover the projected cluster area, given by Eq. (7.7), does not seem to be unrealistic. For example, a wake has been observed behind a massive elliptical galaxy (mass of order $2 \times 10^{12} M_\odot$) moving through the intracluster gas at a speed about $v_c \simeq 1000 \text{ km s}^{-1}$ [34]. The length of the detectable wake is about $X \simeq 130 \text{ kpc}$ (assuming that it lies in the sky plane), and its mean radius is 40 kpc (obtained from the quoted volume of about $2 \times 10^6 \text{ kpc}^3$). The projected area of the wake is about 10^4 kpc^2 , as compared to 10^3 kpc^2 for the wake parameters derived above. This wake has been detected only because it is exceptionally strong, and it is not implausible that weaker but more numerous galactic wakes can cover the projected area of the central parts of galaxy clusters.

We conclude that subcluster wakes are likely to be turbulent, but galactic wakes can be laminar if the viscosity of the intracluster gas is as large as Spitzer's value. Given the uncertainty of the physical nature (and hence, estimates) of the viscosity of the magnetized intracluster plasma, we suggest that turbulent galactic wakes remain a viable possibility. Both types of wake have low volume filling factor but can have an area covering factor of order unity. Parameters of turbulence and magnetic fields produced within the wakes are given in the last two lines of Table 2.

7.4. Magnetic fields in the intracluster gas

Parameters of magnetic fields produced by the fluctuation dynamo at various stages of the cluster evolution are presented in Table 2 [50]. This model implies that the correlation scale of random motions in the intracluster gas, l_0 , is larger than that assumed earlier. With $l_0 \simeq 150$ kpc (Table 2), only 5 turbulent cells occur along a path length of $L = 750$ kpc. The resulting degree of polarization of radio emission from clusters with synchrotron halos can be estimated as $p \simeq \frac{1}{2} p_0 / n^{1/2} \simeq 0.2$, where $p_0 \approx 0.7$, $n \simeq L/l_0$ is the number of magnetic structures along the line of sight (assuming that one magnetic sheet with well-ordered magnetic field occurs in each turbulent cell and that the linear resolution is better than l_0), and a factor 1/2 allows, in a very approximate manner, for the volume-filling magnetic field outside the magnetic sheet which only produces unpolarized emission. Depolarization by Faraday dispersion and beam depolarization can reduce the degree of polarization to a fraction of percent at long wavelengths. However, polarization observations at wavelengths 3–6 cm (where Faraday depolarization is sufficiently weak) can reveal magnetic structures produced by the dynamo action if the angular resolution is high enough.

7.5. Interstellar turbulent magnetic fields

Using parameters typical of the warm phase of the ISM, theory of Sect. 7.1 predicts that the small-scale dynamo would produce magnetic flux ropes of the length (or the curvature radius) of about $l_0 = 50$ – 100 pc and thickness 3–5 pc from Eq. (7.4) for $R_{\text{mc}} = 50$ and $s = 5/3$. The volume filling factor of the ropes is $f \simeq l_0 l_B^2 / l_0^3 \simeq R_{\text{mc}}^{-3/2} \simeq 3\%$ assuming that there is one flux rope per turbulent cell, and $3n\%$ if there are n ropes. The field strength within the ropes, if at equipartition with the turbulent energy, has to be of order $1.5 \mu\text{G}$ in the warm phase ($n = 0.1 \text{ cm}^{-3}$, $v_0 = 10 \text{ km s}^{-1}$) and $0.5 \mu\text{G}$ in the hot gas ($n = 10^{-3} \text{ cm}^{-3}$, $v_0 = 40 \text{ km s}^{-1}$). Note that some heuristic models of the small-scale dynamo admit solutions with magnetic field strength within the ropes being significantly above the equipartition level, e.g., because the field configuration locally approaches a force-free one, $|(\nabla \times \mathbf{B}) \times \mathbf{B}| \ll B^2 / l_B$ [6].

The small-scale dynamo is not the only mechanism producing random magnetic fields (e.g., §4.1 in Ref. [4], and references therein). Any mean-field dynamo action producing magnetic fields at scales exceeding the turbulent scale also generates small-scale magnetic fields. Similarly to the mean magnetic field, this component of the turbulent field presumably has a filling factor close to unity in the warm gas and its strength is expected to be close to equipartition with the turbulent energy at all scales. This component of the turbulent magnetic field may be confined to the warm gas, the site of the mean-field dynamo action, so magnetic field in the hot phase may have a better pronounced ropy structure.

The overall structure of the interstellar turbulent magnetic field in the warm gas can be envisaged as a quasi-uniform fluctuating background with one percent of the volume occupied by flux ropes (filaments) of a length 50–100 pc containing a well-ordered magnetic field. This basic distribution would be further complicated by compressibility, shock waves, MHD instabilities (such as Parker instability), the fine structure at subviscous scales, etc.

The site of the mean-field dynamo action is plausibly the warm phase rather than the other phases of the ISM. The warm gas has a large filling factor (so it can occupy a percolating global region), it is, on average, in a state of hydrostatic equilibrium, so it is an ideal site for both the small-scale and mean-field dynamo action. Molecular clouds and dense clouds of neutral hydrogen have too small a filling factor to be of global importance. The time scale of the small-scale dynamo in the hot phase is $l_0/v_0 \simeq 10^6$ yr for $v_0 = 40$ km s⁻¹ and $l_0 = 0.04$ kpc (the width of the hot, ‘chimneys’ extended vertically in the disc). This can be shorter than the advection time due to the vertical streaming of the hot gas in the galactic fountain flow, $h/U_z \simeq 10^7$ yr with $h = 1$ kpc and $U_z = 100$ km s⁻¹. Therefore, the small-scale dynamo action should be possible in the hot gas. However, the growth time of the mean magnetic field must be significantly longer than l_0/v_0 , reaching a few hundred Myr. Thus, the hot gas can hardly contribute significantly to the mean-field dynamo action in the disc and can drive the dynamo only in the halo [45]. The main rôle of the fountain flow in the disc dynamo is to enhance magnetic connection between the disc and the halo.

8. Conclusions

A remarkable property of systems with high electric conductivity (or large magnetic Reynolds number R_m) is that the decay time of magnetic field due to Ohmic resistivity can be very long. Since astrophysical plasmas usually have extremely large values of R_m , the Ohmic decay time often exceeds the age of the Universe. Does this make dynamos unnecessary? We believe that the answer to this question is negative because astrophysical plasmas are most often turbulent. A fundamental property of turbulence is the energy cascade to small scales (in three dimensions). If magnetic field is weak and $R_m \gg 1$, the turbulent motions will inevitably tangle magnetic fields and the magnetic energy will be transferred from the energy-range scale l to small scales, where Ohmic dissipation is rapid. (In systems with large magnetic Prandtl number, this will be the viscous dissipation scale, where the magnetic Reynolds number can still be large; however, this scale is by far smaller than that of observable astrophysical magnetic fields. If the initial magnetic field has a scale much larger than l , it will be reduced to l at the relatively short turbulent diffusion time.) The time scale of magnetic field decay

is then controlled by the cascade time, i.e., eddy turnover time. If, on the other hand, magnetic field is strong enough, any externally maintained turbulence is not needed as the Lorentz force will induce motions which will become turbulent if the magnetic field is non-homogeneous enough. The magnetically-induced turbulence will then drain its parent magnetic field by dissipating its energy in few eddy turnover times as above. Altogether, any three-dimensional, turbulent, magnetized system must host a dynamo (unless its magnetic field is maintained by external electric currents or decays). Indeed, turbulent flows can drive the large- and small-scale dynamos, but magnetic fields produced by them are controlled by the dynamo mechanism rather than by the initial magnetic field. In this sense, the properties of the initial magnetic field in a turbulent system are unimportant as long as it can provide a suitable seed for the dynamo. In other words, initial conditions are forgotten in a dynamo system (as in any other unstable system) unless the initial magnetic field is strong enough to make the dynamo nonlinear from the very beginning.

Acknowledgements

AS is grateful to Barbara Ferreira, Waleed Mouhali, Adolfo Ribeiro and Christophe Gissinger for their help in removing errors from the calculations presented here. Barbara Ferreira has carefully read the text and made helpful suggestions. Useful discussions with A. Brandenburg and K. Subramanian are gratefully acknowledged. AS thanks the organizers of the Summer School for the privilege to present the lectures, and for financial support. This work was partially supported by the Royal Society and the Leverhulme Trust grant F/00125/N.

References

- [1] H.W. Babcock, Zeeman effect in stellar spectra, *Astrophys. J.* **105**, 105–191 (1947).
- [2] R. Beck, Magnetic fields in normal galaxies, *Phil. Trans. Roy. Soc. London A* **358**, 777–796 (2000).
- [3] R. Beck, Magnetism in the spiral galaxy NGC 6946: magnetic arms, depolarization rings, dynamo modes, and helical fields, *Astron. Astrophys.* **470**, 539–556 (2007).
- [4] R. Beck, A. Brandenburg, D. Moss, A. Shukurov and D. Sokoloff, Galactic magnetism: recent developments and perspectives, *Ann. Rev. Astron. Astrophys.* **34**, 155–206 (1996).
- [5] R. Beck, A. Shukurov, D. Sokoloff and R. Wielebinski, Systematic bias in interstellar magnetic field estimates, *Astron. Astrophys.* **411**, 99–107 (2003).
- [6] M.P. Belyanin, D.D. Sokoloff and A.M. Shukurov, Asymptotic steady-state solutions to the nonlinear hydromagnetic dynamo equations, *Russ. J. Math. Phys.* **2**, 149–174 (1994).

- [7] E.M. Berkhuijsen, C. Horellou, M. Krause, N. Neininger, A.D. Poezd, A. Shukurov and D.D. Sokoloff, Magnetic fields in the disk and halo of M51, *Astron. Astrophys.* **318**, 700–720 (1997).
- [8] J.G. Bolton and J.P. Wild, On the possibility of measuring interstellar magnetic fields by 21-cm Zeeman splitting, *Astrophys. J.* **125**, 296–297 (1957).
- [9] A. Brandenburg and K. Subramanian, Astrophysical magnetic fields and nonlinear dynamo theory, *Phys. Rep.* **417**, 1–209 (2005).
- [10] C.L. Carilli and G.B. Taylor, Cluster magnetic fields, *Ann. Rev. Astron. Astrophys.* **40**, 319–348 (2002).
- [11] T.E. Clarke, P.P. Kronberg, H. Böhringer, A new radio-X-ray probe of galaxy cluster magnetic fields, *Astrophys. J. Lett.* **547**, L111–L114 (2001).
- [12] T.A. Enßlin and C. Vogt, Magnetic turbulence in cool cores of galaxy clusters, *Astron. Astrophys.* **453**, 447–458 (2006).
- [13] P. Frick, R. Stepanov, A. Shukurov and D. Sokoloff, Structures in the rotation measure sky, *Mon. Not. Roy. Astron. Soc.* **325**, 649–664 (2001).
- [14] U. Frisch, *Turbulence. The Legacy of A.N. Kolmogorov*, Cambridge Univ. Press, Cambridge, 1995.
- [15] F. Govoni and L. Feretti, Magnetic fields in clusters of galaxies, *Int. J. Mod. Phys.* **13**, 1549–1594 (2004).
- [16] G.E. Hale, On the probable existence of a magnetic field in sun-spots, *Astrophys. J.* **28**, 315–343 (1908).
- [17] A. Herzenberg, Geomagnetic dynamos, *Proc. Roy. Soc. Lond.* **250A**, 543–583 (1958).
- [18] D.W. Hughes, R. Rosner and N.O. Weiss, eds., *The Solar Tachocline*, Cambridge Univ. Press, Cambridge, 2007.
- [19] A.B. Iskakov, A.A. Schekochihin, S.C. Cowley, J.C. McWilliams and M.R.E. Proctor, Numerical demonstration of fluctuation dynamo at low magnetic Prandtl numbers, *Phys. Rev. Lett.* **98**, 208501 (2007).
- [20] R.M. Kulsrud and E.G. Zweibel, On the origin of astrophysical magnetic fields, *Rep. Prog. Phys.* **71**, 046901 (2008).
- [21] L.D. Landau and E.M. Lifshitz, *Quantum Mechanics. Non-Relativistic Theory*, Pergamon Press, Oxford, 1974.
- [22] L.D. Landau and E.M. Lifshitz, *Fluid Mechanics*, Pergamon Press, Oxford, 1975.
- [23] J. Larmor, How could a rotating body such as the Sun become a magnet? Rep. 87th Meeting Brit. Assoc. Adv. Sci., Bournemouth, 1919 Sept. 9–13, John Murray, London, pp. 159–160.
- [24] C.F. McKee and J.P. Ostriker, A theory of the interstellar medium—Three components regulated by supernova explosions in an inhomogeneous substrate, *Astrophys. J.* **218**, 148–169 (1977).
- [25] K.R. Mecke, T. Buchert and H. Wagner, Robust morphological measures for large-scale structure in the Universe, *Astron. Astrophys.* **288**, 697–704 (1994).
- [26] A.S. Monin and A.M. Yaglom, *Statistical Fluid Mechanics*, Vol. 2, Dover Publ., 2007.
- [27] A.G. Pacholczyk, *Radio Astrophysics. Nonthermal Processes in Galactic and Extragalactic Sources*, Freeman, San Francisco, 1970.
- [28] E.N. Parker, Hydromagnetic dynamo models, *Astrophys. J.* **122**, 293–314 (1955).
- [29] N. Piskunov and O. Kochukhov, Doppler imaging of stellar magnetic fields. I. Techniques, *Astron. Astrophys.* **381**, 736–756 (2002).
- [30] I. Rogachevskii and N. Kleeorin, Intermittency and anomalous scaling for magnetic fluctuations, *Phys. Rev. E* **56**, 417–426 (1997).

- [31] A.A. Ruzmaikin, A.M. Shukurov and D.D. Sokoloff, *Magnetic Fields of Galaxies*, Kluwer Academic Publ., Dordrecht, 1988.
- [32] A. Ruzmaikin, D. Sokoloff and A. Shukurov, The dynamo origin of magnetic fields in galaxy clusters, *Mon. Not. Roy. Astron. Soc.* **241**, 1–14 (1989).
- [33] V. Sahni, B.S. Sathyaprakash and S.F. Shandarin, Shapefinders: a new shape diagnostic for large-scale structure, *Astrophys. J.* **495**, L5–L8 (1998).
- [34] I. Sakelliou, D.M. Acreman, M.J. Hardcastle, M.R. Merrifield, T.J. Ponman and I.R. Stevens, The cool wake around 4C 34.16 as seen by XMM-Newton, *Mon. Not. Roy. Astron. Soc.* **360**, 1069–1076 (2005).
- [35] A.A. Schekochihin and S.C. Cowley, Turbulence, magnetic fields, and plasma physics in clusters of galaxies, *Phys. Plasmas* **13**, 056501–056501-8 (2006).
- [36] A.A. Schekochihin, N.E.L. Haugen, A. Brandenburg, S.C. Cowley, J.L. Maron and J.C. McWilliams, Onset of small-scale turbulent dynamo at low magnetic Prandtl numbers, *Astrophys. J. Lett.* **625**, L115–L118 (2005).
- [37] A.A. Schekochihin, S.C. Cowley, R.M. Kulsrud, G.W. Hammett and P. Sharma, Plasma instabilities and magnetic field growth in clusters of galaxies, *Astrophys. J.* **629**, 139–142 (2005).
- [38] A.A. Schekochihin, A.B. Iskakov, S.C. Cowley, J.C. McWilliams, M.R.E. Proctor and T.A. Yousef, Fluctuation dynamo and turbulent induction at low magnetic Prandtl numbers, *New J. Phys.* **9**, 300 (2007).
- [39] J. Schmalzing and T. Buchert, Beyond genus statistics: a unifying approach to the morphology of cosmic structure, *Astrophys. J.* **482**, L1–L4 (1997).
- [40] J. Schmalzing, T. Buchert, A.L. Melott, V. Sahni, B.S. Sathyaprakash and S.F. Shandarin, Disentangling the cosmic web. I. Morphology of isodensity contours, *Astrophys. J.* **526**, 568–578 (1999).
- [41] A. Shukurov, Introduction to galactic dynamos, in: *Mathematical Aspects of Natural Dynamos*, E. Dormy and A.M. Soward, eds., Chapman and Hall/CRC, London, 2007, pp. 313–359.
- [42] A. Shukurov, D. Sokoloff, K. Subramanian and A. Brandenburg, Galactic dynamo and helicity losses through fountain flow, *Astron. Astrophys.* **448**, L33–L36 (2006).
- [43] Y. Sofue and V. Rubin, Rotation curves of spiral galaxies, *Ann. Rev. Astron. Astrophys.* **39**, 137–174 (2001).
- [44] D.D. Sokoloff, A.A. Bykov, A. Shukurov, E.M. Berkhuijsen, R. Beck and A.D. Poezd, Depolarisation and Faraday effects in galaxies and other extended radio sources, *Mon. Not. Roy. Astron. Soc.* **299**, 189–206 (1998) [Erratum: op. cit. **303**, 207–208 (1999)].
- [45] D.D. Sokoloff and A. Shukurov, Regular magnetic fields in coronae of spiral galaxies, *Nature* **347**, 51–53 (1990).
- [46] S.R. Spangler, A technique for measuring electrical currents in the Solar corona, *Astrophys. J.* **670**, 841–848 (2007).
- [47] M. Stix, *The Sun*, Springer, Berlin, 2002.
- [48] A.W. Strong, I.V. Moskalenko and V.S. Ptuskin, Cosmic-ray propagation and interactions in the Galaxy, *Ann. Rev. Nucl. Particle Sys.* **57**, 285–327 (2007).
- [49] K. Subramanian, Unified treatment of small- and large-scale dynamos in helical turbulence, *Phys. Rev. Lett.* **83**, 2957–2960 (1999).
- [50] K. Subramanian, A. Shukurov and N.E. L. Haugen, Evolving turbulence and magnetic fields in galaxy clusters, *Mon. Not. Roy. Astron. Soc.* **366**, 1437–1454 (2006).
- [51] S. Tobias and N. Weiss, Stellar dynamos, in: *Mathematical Aspects of Natural Dynamos*, E. Dormy and A.M. Soward, eds., Chapman and Hall/CRC, London, 2007, pp. 281–311.

- [52] A.G. Tomboulides and S.A. Orszag, Numerical investigation of transitional and weak turbulent flow past a sphere, *J. Fluid Mech.* **416**, 45–73 (2000).
- [53] G.L. Verschuur, Positive determination of an interstellar magnetic field by measurement of the Zeeman splitting of the 21-cm hydrogen line, *Phys. Rev. Lett.* **21**, 775–778 (1968).
- [54] G.L. Verschuur, Observations of the Galactic magnetic field, *Fund. Cosm. Phys.* **5**, 113–191 (1979).
- [55] S.L. Wilkin, C.F. Barengi and A. Shukurov, Magnetic structures produced by the fluctuation dynamo. *Phys. Rev. Lett.* **99**, 134501 (2007).
- [56] Ya.B. Zeldovich, A.A. Ruzmaikin and D.D. Sokoloff, *The Almighty Chance*, World Sci., Singapore, 1990.